Cover illustration:

Self-repairing concept: Balanced oxygen and H-induced metal cation transport in pretransition Zr-based oxide scales

The present study was performed in the Division of Corrosion Science (Materials Science and Engineering Department) at Royal Institute of Technology, Stockholm, Sweden under the supervision of Ass. Prof. Gunnar Hultquist and Magnus Limbäck, funded by Westinghouse Electric Sweden AB.

ISRN KTH/MSE--06/53--SE+CORR/AVH

ISBN 91-7178-429-2

Abstract

Most metals and alloys in the presence of oxygen and moisture will instantaneously react and form a thin (2-5 nm) surface oxide layer. For further reaction to occur, oxygen ions and/or metal cations often diffuse through the already formed oxide layer. The corrosion resistance of a metal in aggressive environments at high temperatures depends on the properties of the surface oxide scale.

Zirconium-based alloys represent the main structural materials used in water-cooled nuclear reactors. For these materials, the formation of a thin, adherent oxide scale with long-term stability in high temperature water/steam under irradiation conditions, is crucial. In this thesis, the transport of oxygen and hydrogen through Zr-based oxide scales at relevant temperatures for the nuclear industry is investigated using isotopic gas mixtures and isotope-monitoring techniques such as Gas Phase Analysis and Secondary Ion Mass Spectrometry.

Porosity development in the oxide scales generates easy diffusion pathways for molecules across the oxide layer during oxidation. A considerable contribution of molecular oxygen to total oxygen transport in zirconia has been observed at temperatures up to 800°C. A novel method for evaluation of the gas diffusion, gas concentration and effective pore size of oxide scales is presented in this thesis. Effective pore sizes in the nanometer range were found for pretransition oxides on Zircaloy-2. A mechanism for densification of oxide scales by obtaining a better balance between inward oxygen and outward metal transport is suggested. Outward Zr transport can be influenced by the presence of hydrogen in the oxide and/or metal substrate. Inward oxygen transport can be promoted by oxygen dissociating elements such as Fe-containing second phase particles. The results suggest furthermore that a proper choice of the second-phase particles composition and size distribution can lead to the formation of dense oxides, which are characterized by low oxygen and hydrogen uptake rates during oxidation.

Hydrogen uptake in Zr-based materials during oxidation in high temperature water/steam can generate degradation due to the formation of brittle hydrides in the metal substrate. A promising method for the suppression of hydrogen uptake has been developed and is presented in this thesis.

Keywords: Zirconia, Zirconium, Zircaloy, hydrogen and oxygen diffusion, SPP, oxygen dissociating elements, oxidation, dissociation, hydration, CO adsorption, molecular transport, porosity.

Author e-mail address: anghel@kth.se

List of publications

The following papers are included in this thesis:

Paper I **Gas phase analysis of CO interactions with solid surfaces at high temperatures**
C. Anghel, E. Hörnlund, G. Hultquist and M. Limbäck
Applied Surface Science 233, p. 392, 2004

Paper II **Influence of Pt, Fe/Ni/Cr–containing intermetallics and deuterium on the oxidation of Zr-based materials**
C. Anghel, G. Hultquist and M. Limbäck
Journal of Nuclear Materials 340(2-3), p. 271, 2005

Paper III **Gas-tight oxides – Reality or just a Hope**
C. Anghel, Q. Dong, J. Rundgren, G. Hultquist, I. Saeki and M. Limbäck
Proceedings of the International Symposium on High-Temperature Oxidation and Corrosion 2005, Nara, Japan, 30 November – 2 December 2005
Materials Science Forum, 522-523, p. 93, 2006

Paper IV **Effects of hydrogen on the corrosion resistance of metallic materials and semiconductors**
G. Hultquist, C. Anghel, and P. Szakalos
Proceedings of the International Symposium on High-Temperature Oxidation and Corrosion 2005, Nara, Japan, 30 November – 2 December 2005
Materials Science Forum, 522-523, p. 139, 2006

Paper V **A gas phase analysis technique applied to in-situ studies of gas-solid interactions**
C. Anghel and Q. Dong
Submitted to ***Journal of Materials Science***

Paper VI **Isotopic investigation of the transport of oxygen species in Y-stabilized zirconia**
C. Anghel and Q. Dong
Submitted to ***Journal of Chemical Physics***

The papers are referred in the text by their roman numerals.

The following papers, although related to papers I-VI, are not included in this thesis:

Effects of O_2 Dissociation on a porous platinum coating in the thermal oxidation of GaAs
G. Hultquist, M. J. Graham, A. T. S. Wee, R. Liu, G. I. Sproule, Q. Dong and C. Anghel
Journal of the Electrochemical Society, 153(2), pg. G182, 2006

Influence of porous Pt-coatings on the thermal oxidation of GaAs and metallic materials
Q. Dong, G. Hultquist , M. J. Graham , C. Anghel and G. I. Sproule
Proceedings of the ***16th International Corrosion Congress***, Beijing, China, 19-24 September, 2005

Oxygen transport in Zirconia
C. Anghel, Q. Dong and G. Hultquist
Proceedings of the ***13th Scandinavian Corrosion Congress, NKM 13***, Reykjavik, Iceland, 18-20 April, 2004

Table of contents

Chapter 1

Introduction

1.1 Background

Zirconium dioxide (zirconia) is a refractory material with an excellent oxygen ion conducting capability at high temperatures used in a wide range of applications such as Solid Oxide Fuel Cells (SOFC)[1,2], oxygen separation membranes[2,3] and oxygen sensors[2]. It is also known to be an effective thermal barrier coating[4] in gas turbines and jet engines due to its low thermal conductivity and good chemical stability in aggressive environments. When the substrate is Zr itself, the zirconia oxide scales are actually corrosion products of the zirconium oxidation. Despite the fact that corrosion is a destructive process, still a positive effect of this corrosion product has to be considered. As long as the oxide layer acts as a barrier between the metal and the corrosive environment, the metal substrate will be protected against further degradation. The main question is: if naturally formed oxide scales (corrosion products) are more dense and more protective compared to the artificially produced functional/structural ceramics?

Zr-based alloys represent the main structural materials used in water-cooled nuclear reactors. For these materials, the formation of a thin, adherent oxide scale with long-term stability in high temperature water and steam is crucial. The oxidation of Zr-based materials in high temperature oxygen, water and steam has been intensively studied in the last 50 years[5-19]. The oxidation process can be divided into three different stages:

1. In the ***initial stage,*** the oxide film is instantaneously formed on the clean Zr surface already at room temperature with linear oxide growth kinetics, being limited to a few monolayers of highly a disordered non-stoichiometric Zr-oxide (so called “air-formed oxide”)[12,20,21]. There are competing processes taking place during the oxidation even at room temperature. After this initial oxide film formation, further oxidation takes place virtually only at higher temperatures.
2. In the ***pre-transition stage***, the air-formed oxide will be further oxidized with cubic or parabolic kinetics up to an oxide thickness of 2 - 3 μm. The oxide is relatively protective but with a growth stress built up at the metal/oxide interface during oxidation[12]. There are discussions about the duplex character of this pre-transition oxide film: an inner non-stoichiometric zirconium oxide “barrier” layer and an outer stoichiometric ZrO_2 porous layer, but the presence of porosity within this “barrier layer” has been also suggested[22].
3. When the oxide thickness exceeds 2 - 3 μm, the oxidation kinetics changes from parabolic to quasi-linear oxide growth and is defined as the ***post-transition stage***. The oxide scale is characterized by a multitude of defects like cracks and pores[12,19,23,24].

The delimitation of these stages for the oxidation of Zr-based materials is well known, but as long as the mechanisms of defect formation in the growing oxide scale are not well defined, the

species involved in the transport are debated[12]. The way in which species like oxygen and hydrogen are transported through the oxide layer governs the oxidation rate.

There are many parameters which influence the transport mode, such as oxide scale morphology, composition, crystalline phase, porosity, the composition and size distribution of the second-phase particles (SPPs). The deterioration mechanisms of these oxide scales in high temperature water and steam have been studied with a variety of techiniques[9] and a number of models have been elaborated[16-18]. However the overall picture is still not clear. Novel approaches to study these phenomena are now considered to improve the present knowledge.

"Gas-tight oxides - Reality or just a hope?". This sentence expresses by itself our interest to study the growth of oxide scales and to find ways to influence the growth mode aiming to obtain long-term protective oxide scales. Ass. Prof. G. Hultquist developed the so-called "Self-repairing" model[25], which shows that improved balance in the oxide growth results in improved oxides. Previous work within our group has proven that small changes at the metal surface (coating with more catalytically active metals) or in the bulk (addition of hydrogen) can influence the species which will be transported through the oxide layer as well as their transport rate.

1.1.1 The Self-repairing concept

The simple equation for oxidation of a metal Me (Eq.1) is actually quite complex.

$$2xMe + yO_2 \rightarrow 2Me_xO_y \qquad (1)$$

The oxide starts to form at surfaces of the exposed metal. These initial surfaces represent the gas/metal (G/M) interfaces. Due to the formation of the oxide scale, the G/M interface will be replaced by new interfaces: oxide/gas (O/G) and oxide/metal (O/M) interfaces. The oxide will therefore separate the metal from the corrosive environment and for corrosion to proceed, mass and charge transport through the oxide scale must take place. A distinction must be made between the oxidation at low and high temperatures. At room temperature, most metals are covered by a thin oxide layer (thickness of about 2-5 nm)[26]. Electron tunneling due to a huge electric field is responsible for the initial oxide growth. After the air-formed oxide layer reaches thicknesses of 2-5 nm, the electrons cannot tunnel through the oxide scale and the oxidation rate decreases abruptly.

At high temperatures, the oxidation can proceed with different oxide growth modes: by inward oxygen transport (ex. Zr-based materials), by outward metal cation transport (ex. Cr) or by mixed, inward oxygen and outward metal cation transport (ex. Al). These three oxide growth mechanisms are illustrated in Figure 1.

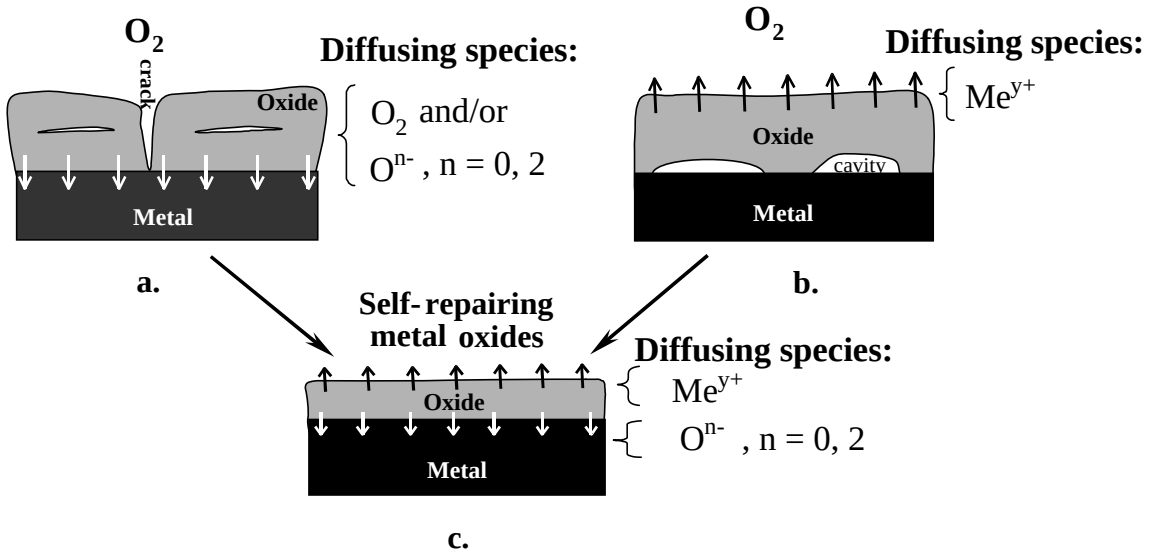

Figure 1. Mechanisms of oxide growth

a. Oxide growth by inward oxygen transport. White arrows represent the oxidation front at the oxide/metal, O/M interface.
b. Oxide growth by outward metal cation transport. Black arrows represent the oxidation front at the oxide/gas, O/G interface.
c. Oxide growth by mixed, inward oxygen and outward metal cation, transport. White and black arrows same as above.

Considering the ***self-repairing concept***, the oxide growth mode should be manipulated towards the mixed transport mode.

For the case of ***inward oxygen transport***, when the volume of the newly formed oxide is larger than the volume of the base metal (Pilling-Bedworth ratio>1), the oxide scale is under compression, and distorted distances between the ions in the oxide lattice are expected (shorter distanced parallel to the O/G interface and longer distanced perpendicular to O/G interface) in comparison to the uncompressed oxide[26]. This distortion can explain stress-induced formation of cracks in the bulk of these oxide scales parallel to the O/G interface, which appear at certain thicknesses. It is also known that these scales can fail due to crack propagation from the oxide surface down to the O/M interface. Improved oxide scales have been obtained by the addition of certain amounts of hydrogen in the environment or in the metal substrate[25]. It has been shown[25] that one of the effects induced by the presence of hydrogen during the oxidation (in the substrate or in the environment) is the increased outward metal cation transport. A possible mechanism is based on a proton-induced high concentration of metal ion vacancies in the oxide scale, which is likely to result in an increased metal ion transport[25].

For the case of ***outward metal cation transport***, during the oxidation, cavities at the O/M interface may form as a result of cation vacancy condensation[26], generating detachment of the oxide scale at certain thicknesses. In this case, a better balance in the oxide growth has been

obtained by the addition of oxygen dissociation elements, such as Pt or rare earth metals, to the base metal[25,27]. The mechanism behind this effect is the increased oxygen dissociation rate at the O/G interface due to these active elements, generating an increased oxygen gradient over the oxide scale and enhanced oxide growth at the O/M interface.

When ***mixed transport*** takes place, the compressive stress in the oxide scale at the O/M interface and in the bulk oxide is reduced by the outward cation transport and the cavity formation is avoided by inward transport of oxygen and oxide formation the O/M interface. The overall result is the formation of a thinner and more protective, gas-tight oxide scale.

1.2 Aim of the thesis

This work aims to improve the knowledge of operating transport mechanisms in oxides on Zr-based materials in various atmospheres. This is done by mainly using an in-situ Gas Phase Analysis (GPA) technique and isotopic gas mixtures combined with other isotope-sensitive techniques such as Secondary Ion Mass Spectrometry (SIMS). This isotopic approach provides the possibility to observe processes which take place during the exposure in-situ by analyzing changes in the gas phase with a mass spectrometer and then attribute them to changes at the surfaces/interfaces as well as in the bulk by SIMS depth profiling.

The application of the "***Self-repairing***" concept to Zr-based materials by engineering of interfaces and surfaces with effects on the overall transport process is considered.

Another aim was is to provide a detailed investigation of the porosity evolution in the oxide scales on Zr-based materials upon exposure to air/O_2 and/or water-containing atmospheres. The formation of a network of open pores in the oxide scales during oxidation and the evolution of their size and distribution are main factors influencing the transport of molecular species and hence crucial for the understanding of the degradation process of these oxide scales.

I.3 References

(1) R. Hansch; D. Lavergnat; N.H. Menzler; D. Stover, *Advanced Engineering Materials* **2005**, *7*, p.142.

(2) A. Mitterdorfer, PhD thesis, Swiss Federal Institute of Technology, **1997**.

(3) P. Pandey; R.S. Chauhan, *Prog. Polym. Sci.* **2001**, *26*, p.853.

(4) K. An; M. Han, *Journal of Materials Science* **2006**, *41*, p.2113.

(5) D. E. Thomas; F. Forscher, *Journal of Metals* **1956**, *8*, p.640.

(6) E.A. Gulbransen; K.F. Andrew, *Journal of Metals* **1957**, p.349.

(7) B. Cox, *Journal of the Electrochemical Society* **1961**, *108*, p.24.

(8) J.L. Whitton, *Journal of the Electrochemical Society* **1968**, *115*, p.58.

(9) A.B. Johnson Jr.; R.M. Horton. Symposium on Zirconium in the Nuclear Industry, **1976**, Quebec, Canada.

(10) D. Arias; T. Palacios; C. Turillo, *Journal of Nuclear Materials* **1987**, *148*, p.227.

(11) E.A. Garcia; G. Bérarger, *Autoridad Regulatoria Nuclear* **1997**, p.1.

(12) *IAEA-TECDOC-996, Viena* **1998**, p.27.

(13) N. Dupin, I. A., C. Servant, C. Toffolon, C. Lemaignan, J.C. Brachet, *Journal of Nuclear Materials* **1999**, *275*, p.287.

(14) Y.P. Lin; Woo, O. T. *Journal of Nuclear Materials* **2000**, *277*, p.11.

(15) P. Tägtström; M. Limbäck; M. Dahlbäck, T. Andersson, H. Pettersson, in: Zirconium in the nuclear industry: 13th International Symposium, **2001**, France, p.96.

(16) S. Abolhassani; M. Dadras; M. Leboeuf; D, Gavillet, *Journal of Nuclear Materials* **2003**, *321*, p.70.

(17) A. Yilmazbayhan, et al., *Journal of Nuclear Materials* **2004**, *324*, p.6.

(18) B. Cox, *Journal of Nuclear Materials* **2005**, *336*, p.331.

(19) A.Yilmazbayhan; E. Breval; A.T. Motta; R.J. Comstock, *Journal of Nuclear Materials* **2006**, *349*, p.265.

(20) A. Lyapin; L.P.H. Jeurgens; E.J. Mittemeijer, *Acta Materialia* **2005**, *53*, p.2925.

(21) S. A. Raspopov, et al. *Journal of Chemical Society Faraday Transactions* **1997**, *93*, p.2113.

(22) N. Ramasubramanian; P. Billot; S. Yagnik. in: Zirconium in the Nuclear Industry: 13th International Symposium, 2001, France, p.222.

(23) A. P. Zhilyaev; J. Szpunar, *Journal of Nuclear Materials* **1999**, *264*, p.327.

(24) M. Tupin, et al., *Materials Science Forum* **2004**, *461-464*, p.13.

(25) G. Hultquist; Tveten, B.; Hörnlund, E.; Limbäck, M.; R. Haugsrud, *Oxidation of Metals* **2001**, *56*, p.313.

(26) R.E. Ulich, *The corrosion and oxidation of metals*; Edward Arnold LTD, **1960**.

(27) G. Hultquist; B. Tveten, B.; E. Hörnlund, *Oxidation of Metals* **2000**, *54*, p.1.

Chapter 2

Zirconium and its alloys

2.1 Survey of Zr-based alloys

Unalloyed zirconium (Zr) was first tested in the 50's in a prototype nuclear reactor for submarines, called STR Mark-1 (Sub-marine Thermal Reactor Mark-1)[1,2]. After this successful early military nuclear project, great efforts were engaged towards the "peaceful uses of atomic energy"[2]. The first commercial power reactor started to be produced in the 60's. The demanding conditions from the nuclear reactors have generated intensive research for material development. Zr has attracted researchers attention as a possible candidate for fuel cladding and pressure tube material due to its low thermal neutron absorption cross-section as well as high corrosion resistance in aggressive environments at high temperatures, good heat transfer and mechanical properties.

Zr is characterized by two crystallographic structures: the low temperature hexagonal closed pack (hcp) structure (α phase) and the high temperature body centred cubic (bcc) structure (β phase)[3]. The α→β allotropic phase transformation takes place at 865°C[3]. The β phase is stable up to 1860°C, which is the melting temperature. The strong anisotropy of the α phase plays an important role in the deformation behaviour of Zr (preferential deformation in longitudinal direction)[3,4].

Unalloyed Zr does not provide sufficient corrosion resistance and mechanical strength for being used in the nuclear reactor core. One of the reasons for this behaviour is the nitrogen impurity present in the Zr substrate (introduced in the Kroll process). Different alloying elements, such as Sn, Ta and Nb have been investigated for the annihilation of the negative effect generated by the nitrogen impurity. ***Sn*** is also characterized by a low neutron adsorption cross-section and thus the first Sn-containing reactor-grade alloy, ***Zircaloy-1*** (Zr 2.5%Sn), was developed[1,3,4,5]. This alloy presented better mechanical properties compared to unalloyed Zr, but the corrosion resistance still needed to be improved. The addition of small amounts (<0.5 wt %) of ***Fe, Ni*** and ***Cr*** to Sn-containing Zr alloys (low tin) that increased the corrosion resistance formed the base for the production of ***Zircaloy-2*** and ***Zircaloy-4*** (Ni free) alloys. The solubility of Fe, Cr and Ni in α-Zr is quite low (< 100 ppm) [6-9], and therefore they form precipitates like $Zr(Fe,Cr)_2$ and $Zr_2(Ni,Fe)$, known as second-phase particles (SPP). It is reported that the distribution of Fe, Cr and Ni within the intermetallic phases affects the dissolution of this particles during irradiation[10]. Parameters like SPP chemical composition, size distribution, density and morphology, all have a great influence on the in-reactor performance of these alloys[10,11]. The development of the Zr-based alloys and their applications[1,3,4] are presented in **Figure 2.1**,.

Zr alloys with **Nb** additions are widely used in Russian nuclear reactors[1,3]. It was found that the addition of Nb reduced the risk for nodular corrosion, lowered the hydrogen uptake and increased the ductility, toughness and resistance to creep. The ***Zr 2.5%Nb*** alloy is used as a pressure tube material in CANDU nuclear power plants (Pressurized Heavy Water Reactor).

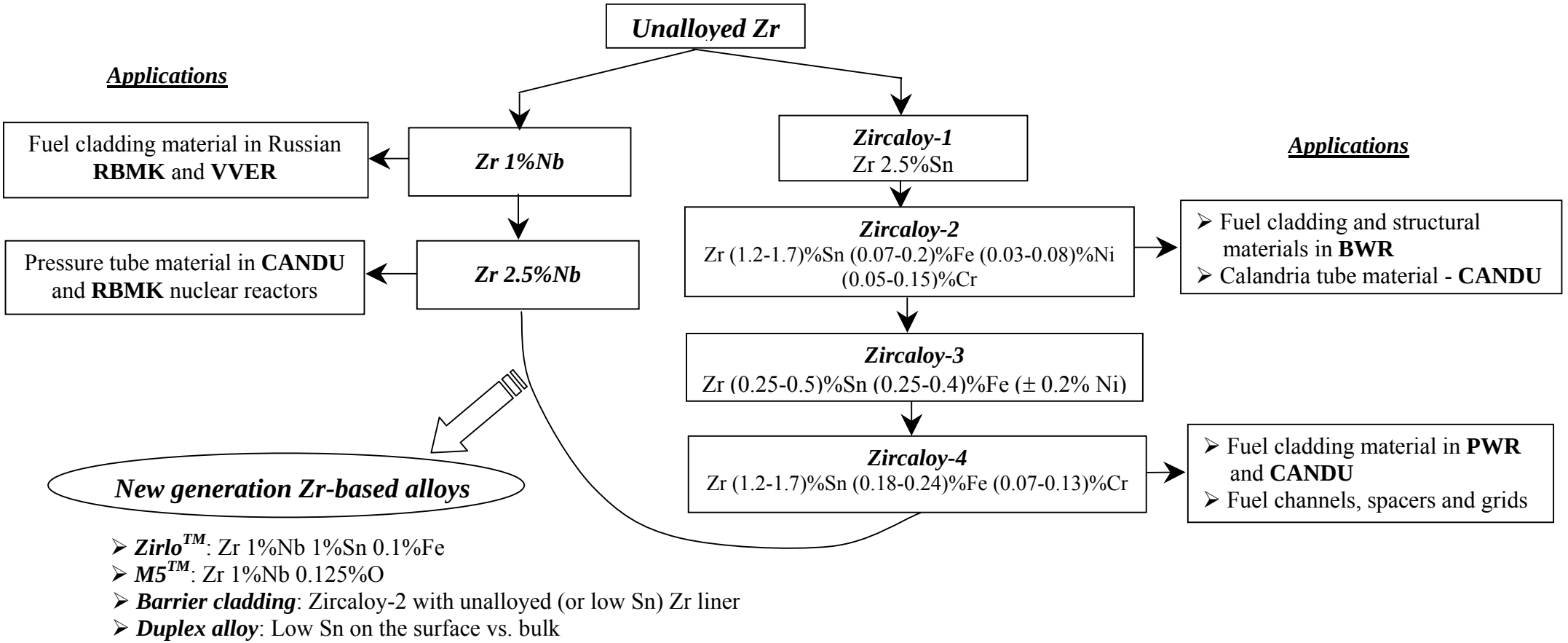

- ***Zirlo***^{TM}: Zr 1%Nb 1%Sn 0.1%Fe
- ***M5***^{TM}: Zr 1%Nb 0.125%O
- ***Barrier cladding***: Zircaloy-2 with unalloyed (or low Sn) Zr liner
- ***Duplex alloy***: Low Sn on the surface vs. bulk

Light Water Reactors, LWR: Pressurized Water Reactor (**PWR**), Boiling Water Reactor (**BWR**),
Reactor Bolshoy Moshchnosty Kanalny or high-power channel reactor (**RBMK**)
Vodo Vodianoi Energheticeskii Reactor or water-water energetic reactor (**VVER**).

Pressurized Heavy Water Reactors: ***PHWR*** also called ***CANDU*** (**CAN**ada **D**euterium **U**ranium).

Figure 2.1 Zr-based alloys: development and applications[1,3,4] (composition in weight %)

Zr has a high affinity for oxygen and therefore, oxygen is an important impurity. ***Oxygen*** is also introduced as an addition element in Zr-based alloys (800-1600 ppm) to increase the yield strength[3]. Oxygen dissolution into the Zr matrix during oxidation, described in more detail in Chapter 2.2, is a crucial process that needs further investigations for an improved understanding of the corrosion mechanisms of Zr-based alloys.

Other elements, such as Al, Mo, C, Si, P, Cu, Hf, N, H, can be present in Zr-based alloys. Due to their impact on the corrosion behaviour, their amount must be kept in ppm range. Among the alloying elements, ***Al, Be, Cd, Hf, N, O, Sn*** and ***Pb*** are *α-stabilizers* and ***Cr, Co, Cu, Mn, Fe, Mo, Ni, Nb, Ag, Ta, Ti, U*** and ***V*** are *β-stabilizers*[3,12]. Oxygen, nitrogen and hydrogen have a strengthening effect on the metal substrate.

The fuel cladding materials have been further optimised for higher burn-up and longer in-reactor operating cycles. Barrier claddings were developed to reduce the pellet-cladding interactions (stress-corrosion cracking) on the fuelside by using an unalloyed (or low Sn) Zr liner. The waterside layer was also optimised (SPP composition, size distribution and Sn content) for improved corrosion resistance in high-temperature water/steam[3,4]. The same concepts were the basis for the development of the Duplex claddings, with good mechanical properties for the inner layer (80% of the total cladding thickness made by Zircaloy 4) and optimised corrosion resistance for the outer layer. The impact of the water chemistry was also considered[3]. The PWR water, maintained at approximately 320°C and 150 bars, contains as main additives: lithium hydroxide, boric acid and dissolved hydrogen[3]. The BWR water/steam is maintained at lower temperature (approx. 290°C) and pressure (70 bar) and additions such as dissolved hydrogen, soluble iron and zinc are generally used[3]. Deliberate hydrogen additions (a few ppm) to the coolant in the Light Water Reactors, LWRs, are aimed to suppress the production of oxygen radicals by water radiolysis. A relatively new approach for BWRs is the use of noble metal chemical addition (NMCA) treatment to reduce the amount of the dissolved oxygen species by catalysing the reaction between these species and the dissolved hydrogen (water production)[13]. By this method, the amount of dissolved hydrogen necessary to maintain a low content of oxygen radicals can be substantially reduced as well as the risk for intergranular stress corrosion cracking. On the other hand, hydrogen is a by-product of the reaction between Zr and water. It is known that a fraction of the produced hydrogen (approximately 20-25% in PWRs and 5% in BWRs in normal conditions) is absorbed by the metal substrate during the oxidation and, due to the low solubility of H in Zr, hydrides start to form[3,10]. To avoid hydride-induced embrittlement of the cladding, a rigorous control of the hydrogen uptake is essential. New Zr-based alloys with better resistance to hydrogen uptake have been selected. In PWRs, the waterside corrosion was improved by reducing the Sn content to < 1.2 wt %[14]. ***Zirlo™***, a Westinghouse quaternary alloy, and ***M5™***, a Framatome alloy, are new mono-claddings with low Sn content, which have better in-reactor performance than the standard Zircaloys[1,3]. In a comparison between Zirlo and Zircaloy-4, Zirlo shows drastic improvements: 55-65% lower

waterside corrosion, 50% lower irradiation growth and 2-5 times lower corrosion in lithiated water[15].

2.2 Oxygen uptake mechanisms

Zirconium has a high affinity for oxygen. Zr-O phase diagram (Fig. 2.2) shows that oxygen can be in solid solution with α–Zr up to 28.6 at. % O at 200°C and its solubility increases with the temperature up to 2065°C (35 at. % O)[3]. During the exposure of Zr to an oxygen-containing atmosphere, an oxygen concentration gradient, from the surface to the bulk metal, will develop. When the solubility limit is exceeded, a surface oxide scale will start to form. The Ellingham diagram (Fig. 2.3) can be used to predict the thermodynamic stability of different oxygen-containing Zr compounds at different temperatures and O_2 pressures.

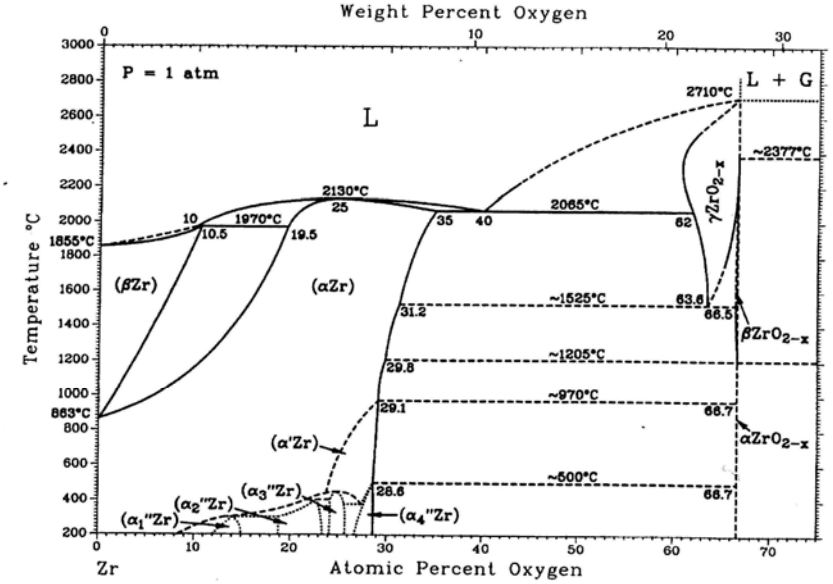

Figure 2.2 Zr-O phase diagram after Massalski[3]

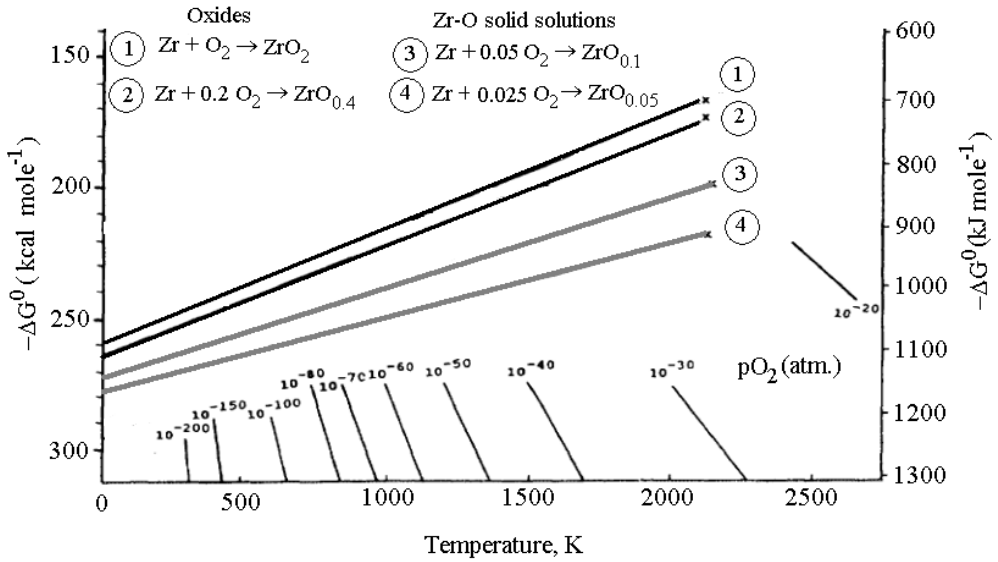

Figure 2.3 Ellingham diagram of Zr-O system modified after Komarek[3]

Oxygen dissolution into the Zr matrix during oxidation can take place because it is thermodynamically more favourable for oxygen to be dissolved in the metal ($ZrO_{0.05}$ and $ZrO_{0.1}$ in Fig. 2.2) than to form the oxide layer[3]. The driving force for the oxidation is the Gibbs free energy change, ΔG^0, corresponding to the reaction between Zr and oxygen. A reaction can occur only if ΔG^0 is negative. When Zr is exposed to an oxygen-containing atmosphere, the oxide will start to form only if the partial pressure of oxygen is higher than the dissociation pressure of the oxide at the temperature of the exposure. This condition is satisfied even in ultra high vacuum and therefore a thin oxide layer (2-5 nm) will always be present on the surface of Zr-based materials. However during exposure to a reducing atmosphere, oxygen can dissolve into the metal substrate diminishing the oxide layer. When a continuous oxide layer is present on the surface, the corresponding oxygen partial pressure at the oxide/Zr(O) interface is equal to the dissociation pressure of the oxide (approximately 10^{-90} atm. at 573K)[3,16]. An oxygen activity gradient is present between the oxide surface and the oxide/Zr(O) interface. The presence of defects in the oxide scale and their type, concentration and structure are influenced by this gradient. Layered structures with different transport behavior could be present in the oxide scale and the effect of impurities or doping could be significant[16]. This gradient can define the thermodynamically stable compounds that might be present within the oxide scale, e.g. stoichiometric ZrO_2 at the oxide/gas interface, non-stoichiometric ZrO_{2-x} at the oxide/Zr(O) interface and Zr-O solid solutions underneath the oxide scale, but since thermodynamic equilibrium is not always reached during the oxidation, kinetic aspects must also be considered. The oxide is highly stressed as a result of lattice parameters mismatch and thermal expansion differences between the oxide scale and the metal[17]. There is a stress gradient across the oxide thickness with a maximum at the oxide/Zr(O) interface and a minimum at the oxide/gas interface[17]. As a result of the high compressive stress, the metastable tetragonal non-stoichiometric Zr-based oxide is stabilized at the oxide/Zr(O) interface[9,10]. Away from the oxide/Zr(O) interface, the tetragonal to monoclinic phase transformation takes place as a result of stress relief with a volume expansion of approximately 7% and generates defects like cracks and pores (easy diffusion pathways)[10]. This transformation can occur inside the barrier layer, possibly inducing porosity within the barrier layer[18]. As long as the mechanisms of defect formation in the growing oxide scale are not well understood, the species involved in the transport are not well defined[10]. Generally, after the formation of a continuous thin (2-5 nm) oxide layer on the Zr surface at elevated temperatures, oxidation proceeds via mass and charge transport. The oxidation can be divided in two stages (Fig. 2.4):

i) a pre-transition stage defined by cubic/parabolic growth kinetics and,
ii) a post-transition stage defined by quasi-linear growth kinetics[3,19,20].

A cyclic behavior in the post-transition stage is generally observed (Fig. 2.4). This can be interpreted as a continuous break down and repair of the oxide scale after the transition. For the overall rate in the post-transition stage, these short cubic cycles can be approximated with a

linear oxidation rate[20,21]. Some of the above mentioned alloys show accelerated corrosion rates at high burn-up. One inflection in the oxidation kinetics in the pre-transition stage, at a thickness of about 0.5-0.7 μm has also been reported[22].

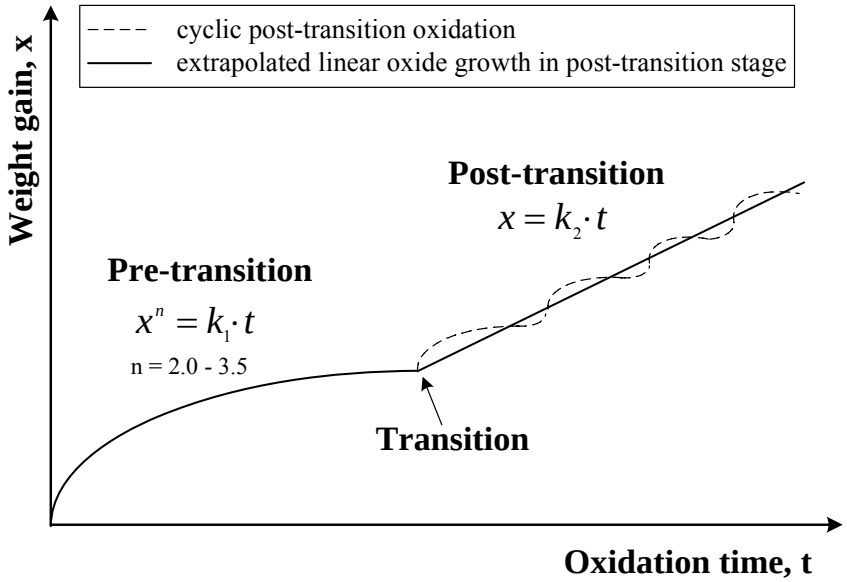

Figure 2.4 Stages in the oxidation of Zr-based materials modified after Gibert[20]. The kinetic equations for the two stages are shown (k_1 and k_2 are the rate constants).

Competing processes take place during oxidation and, for multi-step reactions, the slowest process determines the oxidation rate[23]. The rate-limiting process can change during the oxidation, with a possible change in the oxidation rate. Controversial information is available on this subject for the oxidation of Zr-based materials and thus the identification and analysis of the potential competing processes is presented as follows:

- Oxygen adsorption and dissociation at the oxide/gas interface
- Oxygen spillover via surface diffusion
- Incorporation of oxygen ions into the oxide lattice
- Diffusion of oxygen ions through the oxide scale
- Molecular transport via short-circuit pathways
- Oxygen dissolution into the metal substrate
- Zr cation incorporation into the oxide lattice
- Zr cation outward diffusion
- Electronic transport in the oxide scale

2.2.1 Oxygen adsorption and dissociation at the oxide/gas interface

The processes which can occur at the oxide/gas interface during the exposure of a preoxidized Zr-based alloy to oxygen gas, are illustrated in Figure 2.5. The first stage in the reaction between Zr and oxygen is the physisorption of oxygen. Non-dissociative ***physisorption*** of molecular oxygen, ①, easily takes place as weak van der Waals interactions are involved. This process is fast and reversible (desorption ②). The physisorbed molecules can diffuse via surface diffusion, ③, having a relatively high surface mobility. When the surface adsorption is rate-limiting (at low oxygen partial pressures), a strong dependence of the oxidation rate with the partial pressure of oxygen is observed[16]. ***Chemisorption*** of the physisorbed molecules can occur at defect sites on the surface.

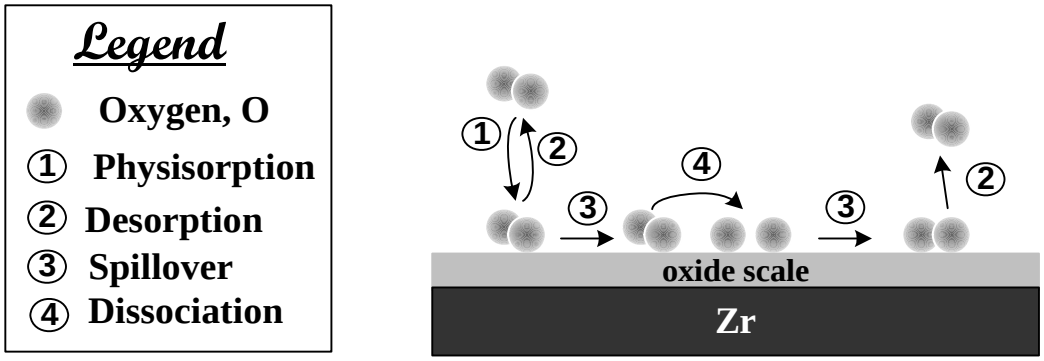

Figure 2.5 Schematic representation of the adsorption/desorption and dissociation of molecular oxygen at the oxide/gas interface of a preoxidized Zr-based alloy

Chemisorption of oxygen is a thermally activated process (for thicker oxides than 2-5nm). The formation of charged species such as O_2^-, O_2^{2-}, O^- and O^{2-} has been reported for oxygen[24]. Electronic transfer from the oxide scale to oxygen atoms/molecules leads to the formation of these charged species. This process can also be rate-limiting, due to the insulating properties of zirconia. The dissociation of an oxygen molecule into oxygen atoms, ④, is illustrated in Figure 2.5. This process is reversible but the recombination rate can be suppressed due to the high reaction rate with Zr. The dissociation rate on preoxidized Zr alloys slowly decreases with increasing oxide thickness, due to an ageing effect. The oxide is growing mainly by inward oxygen transport, and therefore the outer surface may rearrange towards the minimum energy configuration. Impurities or dopants can segregate on the surface of zirconia, locally changing the defect concentration[25]. By engineering of the interfaces, the oxidation properties of Zr-based materials could be controlled. Zirconia is a very good oxygen ion conductor at high temperatures. The presence of mobile oxygen ions is clearly necessary for ionic transport to occur. Raspopov et al.[26] have investigated the initial oxidation of Zr by atomic and molecular oxygen at 873-1123K. Enhanced oxidation has been observed in atomic oxygen (dissociation step was eliminated) at all temperatures investigated. Similar results have been obtained by Iltis

et al.[27] during the exposure of Zircaloy-4 to atomic oxygen containing gas at 520-620K. In both cases[26,27], the investigations were performed for thin films, for which this process could be followed. As the thickness of the oxide scales increases, the differences between the oxidation in molecular O_2 and atomic O-containing gas is less pronounced and it is hence difficult to make straightforward conclusions[27,28]. Enhanced oxidation has also been observed during autoclave experiments in water/steam containing different amounts of dissolved oxygen as well as inside the reactor when the amount of dissolved oxygen, formed by water radiolysis, exceeded the recommended values[3]. Coating of pure zirconium (hydrogen removed by outgassing) with a thin porous layer of Pt induces an increased oxidation rate and growth of thicker and less protective oxide scales (**Paper II**). All these evidences suggest that a rate-limiting step in the oxidation of Zr-based materials at relevant temperatures for the nuclear industry is located at the outer interface. At certain thicknesses, the dissociation of oxygen is the major process, which controls the kinetics of oxide growth. In the case of zirconium alloys, each alloying element has certain effects on the oxidation and it seems plausible that one effect is related to the efficiency for oxygen dissociation.

In **Paper II**, an analysis of oxygen dissociation on preoxidized Zr-based materials and Pt is presented. The results show that oxygen dissociation efficiency decreases in the order: $Pt > Zr_2Fe > Zr_2Ni > ZrCr_2 \geq$ Zircaloy-2 at temperatures around 400°C.

2.2.2 Oxygen spillover via surface diffusion

The spillover term comes from heterogeneous catalysis and describes the movement of active oxygen species O^{n-}, (n = 0, 1, 2), from the active sites for dissociation, such as Pt particles, to absorption sites on the surface[29]. In Figure 2.6, the spillover of dissociated oxygen from a Pt/SPP particle to the adjacent oxide scale is illustrated.

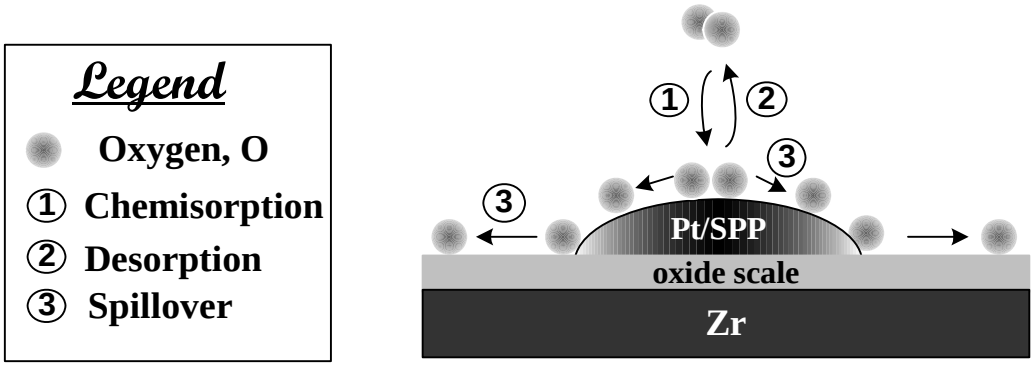

Figure 2.6 Schematics of oxygen spillover from an active area for O_2 dissociation (Pt/SPP particle)

Dissociative adsorption of oxygen, ①, takes place on the active Pt/SPP particle surface. The catalytic activity of these particles is 100 to 10^5 times higher than the activity of the oxide

surface at 400°C as shown in **Paper II**. The resulting active species can recombine and leave the surface in molecular form, ②, or be transported away form the Pt/SPP particles via surface diffusion (spillover ③). An oxygen activity gradient is created on the oxide surface with mm-range effect at temperatures around 400°C. This gradient is also induced in depth through the underlying oxide scale and therefore non-uniform oxide scales can develop.
In BWR type of nuclear reactors, enhanced local corrosion (nodular corrosion) was observed in systems where initially large size SPPs or agglomerated small size SPPs were present[10].

2.2.3 Incorporation of oxygen ions into the oxide lattice

Oxygen ions produced at the oxide surface can be incorporated into the oxide lattice via defect sites. The concentration of these defects at the surface clearly defines the rate of oxygen incorporation. Doping of zirconia with lower valence cations such as Y^{3+}, Fe^{2+}, Fe^{3+}, Ni^{2+}, Cr^{3+} will induce the formation of oxygen vacancies to maintain charge neutrality and will thus determine the main type of mobile defects. Goff et al.[30] have reported that the defect distribution is rather complex, and strongly depending on the dopant concentration and temperature. Fergus[31] suggested that the size of the dopant ion influences the defect association energy. Oxygen vacancies are preferably located near smaller cations (in the case of YSZ, Zr is smaller than Y). Similar results have been reported by Stafford et al.[32] for cubic zirconia doped with lager cations. These large cations can segregate to interfaces and surfaces as a result of the strain energy[33]. Oxygen ions can be trapped due to the formation of defect clusters thus lowering the ionic conductivity. Doping with smaller cations than Zr^{4+} (Ni^{2+}, Fe^{2+}, Fe^{3+}, Cr^{3+}, Sn^{4+}) generates a competition for the oxygen vacancies and local perturbations are expected[34,35]. As shown in Chapter 2.1, Fe, Cr and Ni are common addition elements in Zr-based alloys, which have low solubility in α-Zr and form intermetallic precipitates. Abolhassani et al.[36] found that after the uppermost precipitates start to oxidise, the surface oxide, above the respective precipitates, became depleted in Zr, showing a lens-type feature. This is due to the outward diffusion of Fe (and to lower extent Cr) probably via grain boundaries, which will then be oxidised at the oxide/gas interface. This shows that the distribution of these elements at/near the surface differs significantly from the bulk oxide (where they are incorporated as unoxidized intermetallic particles). Space charge effects at the oxide/gas interface may therefore strongly influence the incorporation of oxygen ad-atoms as well as the transport of the incorporated oxygen ions[37]. Two opposing effects are the result of the presence of Fe, Cr and Ni at the surface: increased oxygen dissociation rate and enhanced space charge effects.

Oxygen exchange between oxygen ad-atoms and lattice oxygen ions also occurs, with an increasing rate of exchange at higher temperatures.

2.2.4 Diffusion of oxygen ions through the oxide scale

The transport of incorporated oxygen ions through the oxide layer takes place via point defects (oxygen vacancies or interstitials), line defects (dislocations) and plane defects (grain boundaries)[38,39]. The transport rate depends on the availability and mobility of these defects. For oxide scales thicker than approximately 5 nm, the driving force for oxygen transport is the oxygen activity gradient across the oxide scale. Wagner's theory predicts a parabolic oxide growth when the rate-limiting step in the oxidation is diffusion of oxygen ions via oxygen vacancies[39]. For Zr-based alloys[22], the growth kinetics in the pre-transition stage is cubic up to approximately 0.5-0.7 μm. This means that other contributions than the transport of oxygen ions to the overall transport must be considered[20,39]. Madeyski et al.[40] pointed out the importance of the short-circuit diffusion processes during the oxidation of Zr even for parabolic kinetics at temperatures up to 862°C. A high dislocation density has been observed in Zircaloy-4 oxide scales obtained under PWR conditions[41]. This can generate increased ionic conductivity as shown by Otsuka et al.[42] for YSZ. High compressive stress as well as irradiation during oxidation can generate these dislocations.

Concerning oxygen diffusion via grain boundaries, differences of several orders of magnitude between grain boundary conductivity and the conductivity inside the grains have been reported (grain boundary diffusion >> diffusion via/in grains)[39]. An oxide scale with fine grains shows high grain boundary conductivity. For oxide scales grown on Zr-based alloys at temperatures around 400°C, two crystallographic phases of zirconia have been reported: monoclinic and tetragonal. The monoclinic phase is stable at low temperatures and is, as expected, the dominating phase in the oxide scale. The tetragonal phase can also be found close to the oxide/Zr(O) interface (stabilized by the high compressive stress and grain size < 30nm) and within the oxide scale near the interface between the partially oxidized intermetallics and the bulk oxide (stabilized by doping of zirconia with lower valence cations which diffuse outward from the intermetallics). The oxygen vacancy concentration in zirconia, which influences the transport of oxygen through the oxide lattice, is higher in the tetragonal phase[43] (2-3 mol %) than in the monoclinic phase (<2 mol %). The tetragonal $\rightarrow$ monoclinic phase transformation takes place with a volume increase of about 7% and has a significant impact on the corrosion behavior of Zr-based alloys[44]. A mixture of large columnar grains, growing perpendicular to the oxide/Zr(O) interface, and small equiaxed grains have been found in the oxide scale. The columnar grains have monoclinic structure[41] and are usually referred as the protective part of the oxide scale[21]. The equiaxed grains show defects like cracks in their grain boundaries[41]. Accelerated corrosion is usually correlated with the increase in the amount of equiaxed grains at the oxide/Zr(O) interface[45,46].

Many researchers[5,47-50] have calculated the diffusion coefficient of oxygen in zirconia using different experimental techniques. A scattering of the diffusion data is mainly observed at low temperatures as shown in Figure 2.7. Values close to the upper limit are usually grain boundary diffusion data and the lower limit data are bulk diffusion data. The diffusion in tetragonal zirconia is faster compared to monoclinic zirconia, but in the oxide scales, an intermediate value is commonly found. The steady state condition is not always obtained, and thus the equilibrium conditions cannot be assumed.

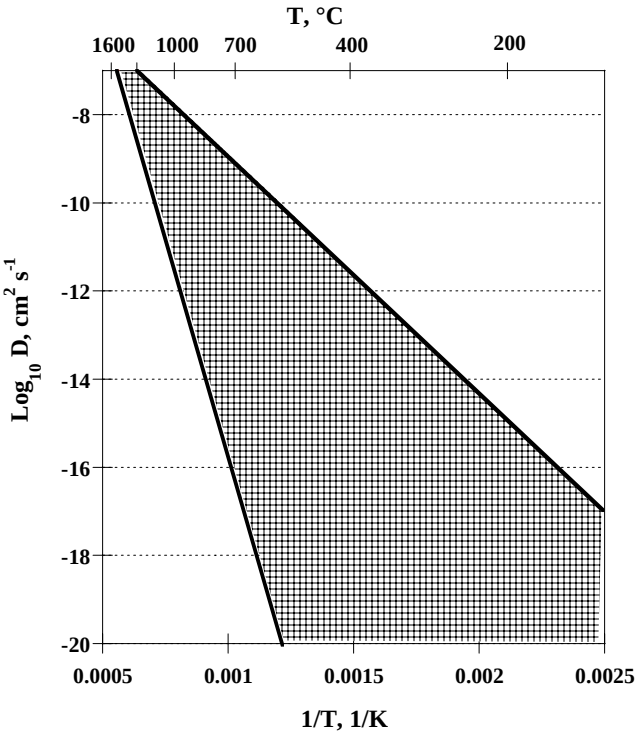

Figure 2.7 Range of diffusivity values, D, as found in the literature for oxygen transport in zirconia[5,47-50]

During the oxidation, the oxide scales are in a continuous transformation including grain growth, phase transformation, porosity development and thickening. All these parameters influence the kinetics of the oxide growth.

2.2.5 Molecular transport via short-circuit pathways

The rate of metal consumption in corrosion is dramatically dependent on the transport of species like oxygen and hydrogen through the oxide layer. This means that defects like open pores can have a considerable influence on the corrosion rate. Even pores of nm-size and their abundance, distribution and interconnectivity may affect the corrosion rate. Naturally when a gas-tight barrier is required, the size of the interconnected pores needs to be smaller than the size of the diffusing molecules. Zr-based alloys form oxide scales up to thicknesses of approximately 2.5-3 μm with an initially cubic oxidation rate followed by a parabolic rate and thus it is

generally assumed that the pre-transition oxide scales are relatively dense. After the kinetic transition, the oxide growth proceeds with a linear rate due to the loss of the oxide scale protectiveness. Pores and cracks in the post-transition scales are easily detected with techniques such as mercury porosimetry, SEM, TEM but not much is known about the evolution of the open porosity before transition as this implies nanometer scale investigations at high temperatures. There are evidences showing that pores exist in these presumably dense oxide scales. Using isotope exchange experiments on pretransition oxides, Ramasubramanian et al.[51] evaluated a pore density in the order of 10^9 cm^{-2} and a pore volume fraction of 0.001% for a 0.2 μm oxide layer (boron concentration was used as an indicator for a pore size of 1 nm). They interpreted this as a very dense oxide scale (almost 100%) but with a high density of micropores[51].

In this thesis, **Paper III** describes an in-situ method to estimate average pore diameters in microporous oxides with and without substrate. In **Paper IV** we found a significant contribution of molecular oxygen to the net oxygen transport in Zirconia ceramics at temperatures lower than 800°C.

2.2.6 Oxygen dissolution into the metal substrate

As shown above in Figure 2.3, the formation of Zr-O solid solutions is thermodynamically more favourable than the formation of the oxide compounds[3]. In Figure 2.2 it could be seen that α-Zr has a high solubility limit for oxygen (approximately 28.6 at% O at 500°C). Oxygen present in the Zr matrix increases the stability range of the α-phase as well as the melting temperature. When the solubility limit is exceeded, the oxide layer will start to form[26]. Inside the metal, oxygen is randomly distributed in octahedral interstitial positions up to a concentration of $ZrO_{0.33}$.[16,39] Yilmazbayhan et al.[21] identified the formation of ordered suboxides (Zr_3O) at the oxide/Zr(O) interface underneath the oxide, ahead of the oxidation front, by using microbeam synchrotron radiation diffraction. Oxygen uptake has a hardening effect on the Zr matrix. Using a combination of microhardness measurements and nuclear reactions of oxygen, Cox[3] has found that the extent of oxygen dissolution increases with the temperature. At temperatures around 400°C, less than 10% of the reacting oxygen is expected to dissolve into the metal substrate. Cox[3] proved experimentally that preferential dissolution of oxygen, from the already formed oxide layer, takes place along the grain boundaries of Zr accompanied by the formation of arrays of pores in the oxygen-depleted grain boundaries (oxide) just above the metal substrate. These defective grain boundaries are possible open porosity development sites. The depth of oxygen penetration inside the metal substrate depends on the oxidation rate and the exposure time. A more shallow oxygen distribution underneath the oxide scale has been observed for rapidly growing oxide scales resulting also in increased brittleness. Lyapin et al.[52] reported that

the diffusivity of oxygen in α-Zr increases considerably at temperature above 523K. By investigating the oxide dissolution rate on α-Zr(1%Nb) and β-Zr(20%Nb), Zhang et al.[53] proposed the following expressions for the diffusion coefficient of oxygen (activation energy in kJ):

Oxygen diffusivity[53] in α-Zr(1%Nb) at 300-450°C:

$$D = 0.172 \exp(-187.47/RT), \quad [cm^2\ s^{-1}] \qquad (1)$$

Oxygen diffusivity[53] in β-Zr(20%Nb) at 175-275°C:

$$D = 0.69 \exp(-149.45/RT), \quad [cm^2\ s^{-1}] \qquad (2)$$

where,

R is the universal gas constant, 8.314 J K^{-1} mol^{-1}, and T is the absolute temperature, K.

Oxygen diffuses much faster in β-Zr(20%Nb) compared to α-Zr(1%Nb). The same behaviour has been observed for α and β Zr and Zircaloys[16,54,55]. This shows that oxide scales formed on β-phase alloys are more susceptible for dissolution. Cox et al.[56] published a comprehensive study of oxygen diffusion in Zr-based alloys.

2.2.7 Zr cation incorporation into the oxide lattice and outward diffusion

To obtain a balance in the oxide growth, both oxygen ions and metal cations need to be involved in the transport. It is well known that Zr is growing mainly by inward oxygen transport, but the contribution of the outward Zr transport cannot be neglected. The outward Zr cation transport via cation vacancies during oxidation of Zr was already taken into consideration in the early 50's by Gulbransen[57]. Lyapin et al.[52] have shown an enhanced outward diffusion of Zr and growth of stoichiometric ZrO_2 at the oxide/gas interface in the temperature range of 100-500°C for very thin oxide films under strong electric fields. Self-diffusion of Zr in zirconia (stabilized with Y_2O_3 or CaO) was investigated using isotopic markers (^{96}Zr) especially at high temperatures and compared with computer simulation results[58-61]. Activation enthalpies of 4-6 eV have been reported for self-diffusion of Zr^{4+} in zirconia at high temperatures. This suggests that the Zr outward diffusion might be negligible at low temperatures, but as shown above, enhanced transport can be induced. The presence of hydrogen in the exposure environment, or in a metal substrate, may increase the outward diffusion of metal cations by reducing the activation enthalpy for the creation and migration of cation vacancies[62-64]. For an optimized hydrogen content, improved adhesion and densification of oxide scales growing mainly by inward oxygen transport has been observed[62]. Two-stage oxidation of metals, first in normal oxygen (^{16}O) followed by exposure to ^{18}O-containing oxygen gas can be used to identify the oxide growth mode. Depth profiling using SIMS is used to identify where the oxide is growing

(following the location of ^{18}O). Using this approach, the effect of hydrogen (D) and Pt on the oxide growth on Zr upon exposure to 20 mbar O_2 at 400°C has been investigated within this thesis (**Paper II**). A small but significant H-induced outward diffusion of Zr was observed in these experiments. The overall oxidation rate was lowered by the presence of hydrogen in the Zr substrate.

2.2.8 Electronic transport in the oxide scale

Formation of oxygen ions that can be incorporated into the oxide lattice is highly dependent on the charge transfer from the oxide to the adsorbed oxygen species. Pure zirconia is an insulator with a wide band gap (5.2 eV)[24]. Additional energy levels (acceptor and/or donor) can be introduced by impurities or dopants[65]. Hydrogen has a beneficial effect on the electronic conduction in zirconia because it easily donates electrons. Nishizaki et al.[66] have shown that hydrogen doping generates a new impurity level below to the conduction band of zirconia reducing significantly the band gap energy[66]. Enhanced electronic transport in Zr-based oxide scales has been obtained by using a Pt wire to short-circuit the oxide surface with the Zr substrate[67]. The results showed an enhanced oxidation rate in oxygen gas at 700-800°C with a change in kinetics from a cubic to a parabolic law. Doping Zr with Fe, Cr and Ni induces a similar effect due to the formation of second-phase particles (SPPs). This is valid for Zircaloy oxide scales as long as the SPPs remain un-oxidized and in contact with both the Zr substrate and the oxidation environment. A degradation of the oxide scale is often associated with the total oxidation of second-phase particles. Increased electronic conductivity in Zr-based oxide scales under γ-photon irradiation is a known process. This "radiation-induced conductivity"[9] can occur during operation conditions in nuclear power plants.

2.3 Hydrogen uptake mechanisms

The waterside corrosion of structural materials used in water-cooled nuclear reactors is significantly influenced by hydrogen uptake. Hydrogen accumulates in the metal substrate and forms solid solutions with the Zr metal until the hydrogen content reaches the solubility limit. Further hydrogen uptake generates the precipitation of hydrides, and as a result, hydrogen embrittlement may occur[51,68,69]. Hydrogen solubility in zirconium at different temperatures has been extensively studied[70-73]. A summary of available data is presented in Figure 2.8.

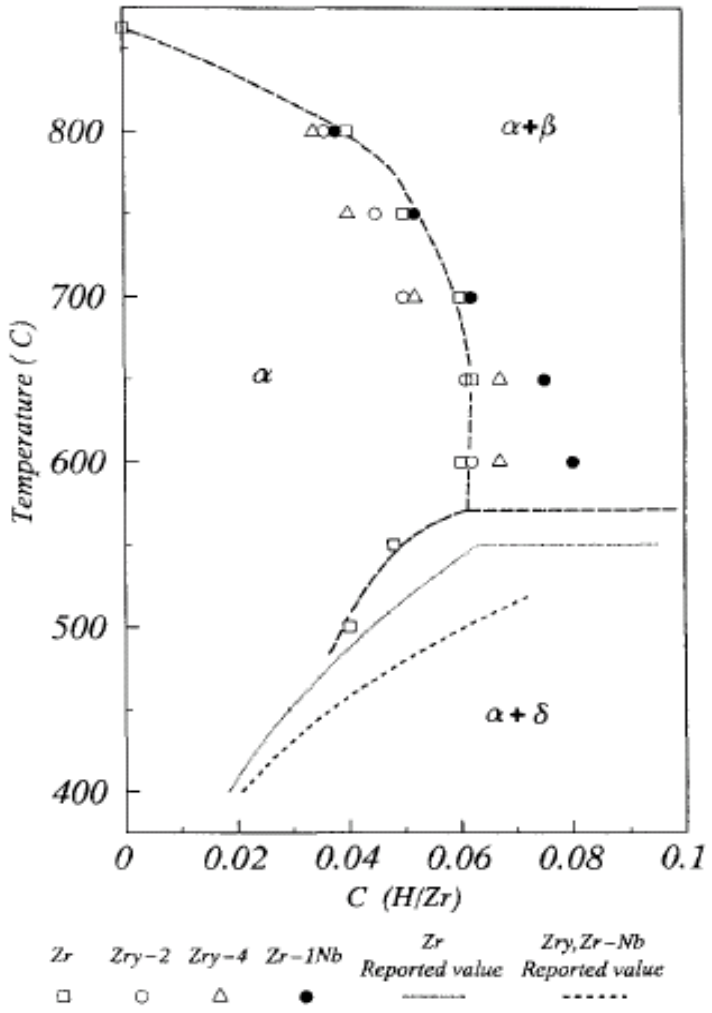

Figure 2.8 – Hydrogen solubility in Zr, after Yamanaka et al.[73]

As illustrated in Fig. 2.8 the presence of alloying elements in the Zr matrix influences the solubility of hydrogen[74]. This might cause problems for example in fuel claddings in which the liner is made by a different Zr alloy. Takagi et al.[75] have studied the redistribution of hydrogen in Zr-lined Zircaloy-2 claddings. They suggested that a significant amount of hydrogen is moving from Zircaloy-2 to Zr during slow cooling, although the difference in their hydrogen solubility limit is quite small. Among the addition elements, Ni and Fe show higher hydrogen

uptake rates compared to Zr, and therefore Zircaloy-4 (containing Fe and Cr but no Ni) shows better resistance against hydrogen uptake than Zircaloy-2 (containing Ni, Fe and Cr)[3].

Hydrogen solubility in Zr also depends on the amount of dissolved oxygen present in the substrate[76,77]. For evaluation of the hydrogen solubility in Zr-O solid solutions, the Zr-O-H ternary system can be used (exemplified in Figure 2.9 for 700°C)[76]. At 700°C, for low oxygen content, the solubility of hydrogen in the α phase increases and then decreases at higher oxygen content[76,78].

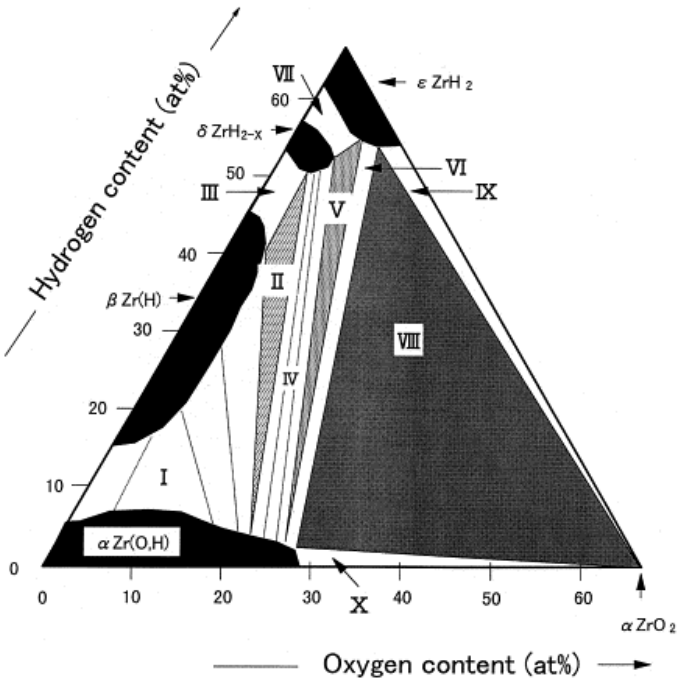

I. $\alpha + \beta$

II. $\alpha + \beta + \delta$

III. $\beta + \delta$

IV. $\alpha + \delta$

V. $\alpha + \delta + \varepsilon$

VI. $\alpha + \varepsilon$

VII. $\delta + \varepsilon$

VIII. $\alpha + \varepsilon + ZrO_2$

IX. $\varepsilon + \alpha\ ZrO_2$

X. $\alpha + \alpha\ ZrO_2$

Figure 2.9 - Isothermal Zr-O-H ternary system at 700°C, after Miyake et al.[76]

It is reported in the literature[77] that hydrogen atoms are preferably located in tetrahedral interstitial sites in Zr-H solid solutions. The radius of these sites (~ 0.036 nm) is about the same as the radius of the hydrogen atom (~ 0.04 nm), which means that the strain induced by hydrogen dissolution in Zr is negligible[77]. Zhang et al.[77] have found that hydrogen tends to segregate to surfaces and interfaces (grain boundaries, cracks and other defects) in Zr. These hydrogen-rich areas are possible nucleation sites for hydrides. When dissolved oxygen is present in the Zr substrate, hydrogen segregation to the Zr surface is enhanced[77]. The concentration of dissolved oxygen in Zr varies from the bulk to the metal/oxide interface and is much higher underneath the oxide, accommodating also more hydrogen in this area. This accumulation could explain the frequently observed deterioration of the "barrier" layer. However, this shows that Zr could diffuse easier outwards when hydrogen is present at the oxide/metal interface. An optimum amount of hydrogen present at this interface could actually be beneficial, supporting the self-repairing process[62].

The diffusivity of hydrogen in Zr-based materials has been intensively studied at relevant temperatures for the nuclear industry[70,72,77]. Sawatzky[70] proposed the following expression for hydrogen diffusivity in Zircaloy-2 (α-phase) at 260-560°C (activation energy in cal/mol):

$$D = 2.17 \times 10^{-3} \exp(-8380/RT), \quad [cm^2\ s^{-1}] \quad (3)$$

where,

R is the universal gas constant, 1.987 cal K^{-1} mol^{-1}, and T is the absolute temperature, K.

Hydrogen could originate from internal and/or external sources. Internally, a direct contact between Zr and other metals, could result in hydrogen uptake, when a hydrogen activity gradient is present[3]. Hydrogen gas present in the environment and/or obtained as a by-product of the $Zr + H_2O$ reaction can be considered as an external source of hydrogen[3]. In this case, hydrogen (water) diffusion through the oxide scale is a prerequisite for hydrogen uptake in the metal substrate. The hydrogen transport properties of the oxide layer (corrosion product of Zr in reaction with oxygen/water/steam) are thus very important.

Using a thermal desorption technique, Miyake et al.[76] have found that the solubility of hydrogen is in the range of 10^{-5} – 10^{-4} mol H/mol oxide in monoclinic zirconia at 500-1000°C. This solubility decreases with increasing temperature. A summary of literature data on hydrogen solubility in different oxides is presented in Figure 2.10.

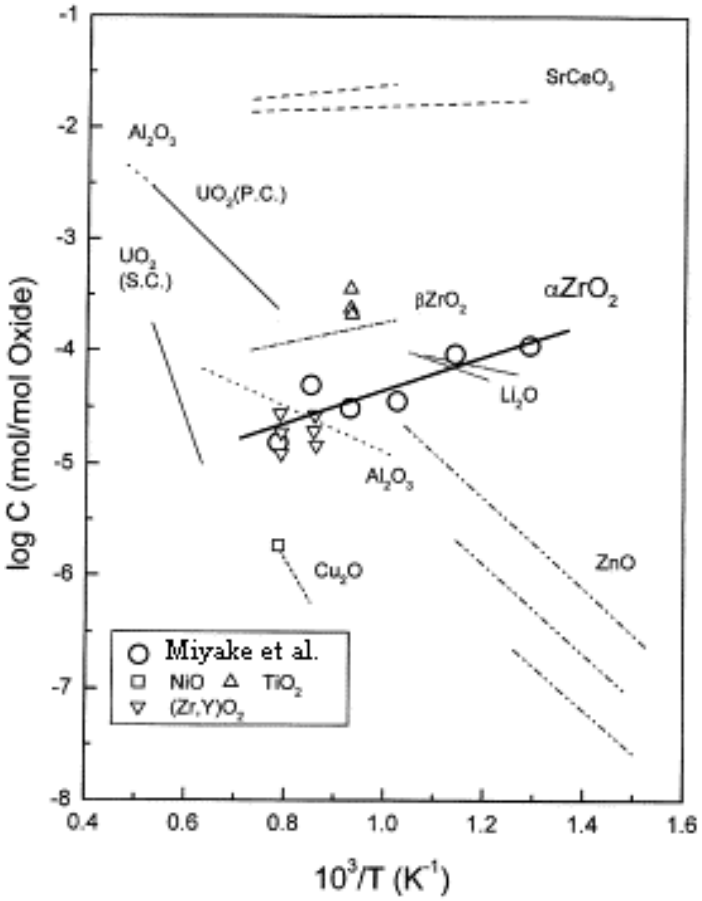

Figure 2.10 – Hydrogen solubility in some oxides versus 1/T, after Miyake et al.[76]

Figure 2.10 shows that the solubility of hydrogen in tetragonal zirconia (β ZrO_2) is higher than in monoclinic zirconia (α ZrO_2). It has been suggested that the diffusion of hydrogen in Zr-based oxide scales depends on the fraction of the tetragonal ZrO_2 present in the oxide scale[79].

Khatamian et al.[80] have studied the diffusivity of hydrogen in oxide scales grown on pure Zr and Zr-2.5% Nb alloy for temperatures up to 700°C. Higher hydrogen diffusion rates in the Zr-2.5% Nb oxide scales have been observed[80]. Using tracer-based measurements[80], the following expressions for the diffusion coefficient of hydrogen in pretransition oxide scales (thickness of ~1μm) on pure Zr and on Zr-2.5%Nb have been proposed (activation energies in kJ/mol) at temperatures up to 700°C:

Hydrogen diffusivity[80] in oxide scales on pure Zr:

$$D = 1.13 \times 10^{-12} \exp(-100.1/RT), \quad [m^2\ s^{-1}] \qquad (4)$$

Hydrogen diffusivity[80] in oxide scales on Zr-2.5%Nb:

$$D = 3.05 \times 10^{-13} \exp(-53.7/RT), \quad [m^2\ s^{-1}] \qquad (5)$$

where,

R is the universal gas constant, 8.314 J K^{-1} mol^{-1}, and T is the absolute temperature, K.

To compare the diffusivity of hydrogen in Zr-based alloys and in the oxide layers grown on these materials, the diffusivity values calculated using the above-mentioned expressions (3-5) for 400°C are presented in Table1.

Table 1. Diffusivity data for hydrogen in Zr-based materials at 400°C: metal/alloy and oxide scales

Material		***D ($cm^2\ s^{-1}$)***	***Method***	***Expression / Ref.***
Zr and Zircaloy	Polycrystalline α Zircaloy-2	4.1×10^{-6}	Hot extraction	(1) Sawatzky[70]
	Polycrystalline Zr	2.8×10^{-6}	Tracer-based	Khatamian et al.[80]
Oxide scales	Polycrystalline 1 μm oxide layer on pure Zr	1.9×10^{-16}	Tracer-based	(2) Khatamian et al.[80]
	Polycrystalline 1 μm oxide layer on Zr-2.5% Nb	2×10^{-13}	Tracer-based	(3) Khatamian et al.[80]

From the table it can be concluded that the diffusion of hydrogen in metallic substrates is much faster than in pretransition oxide scales. The mechanisms for hydrogen transport through Zr-based oxide scales have been investigated using hydrogen isotopes and isotope-tracing techniques such as SIMS[18,81], ion-beam implantation[80], permeation measurements combined

with mass spectrometry[18,82,83] and nuclear analysis[84]. These studies revealed that, for thin oxide layers formed on Zr alloys, the un-oxidized second-phase particles, SPPs, have a significant effect on the hydrogen transport as long as they interconnect the metal substrate with the exposure environment. The SPPs have a high affinity for hydrogen and act as short-circuit pathways for hydrogen transport through the oxide scale[85]. Hydrogen can easily diffuse through these thin oxide scales via metallic SPPs towards the metal substrate, or outward (vacuum extraction). The diffusion direction is defined by the activity gradient of hydrogen across the oxide scale. As the oxidation proceeds, the thickness of the oxide scale exceeds the size of the SPPs, which also will become oxidized. The SPPs cannot mediate the transport anymore and thus the hydrogen transport rate decreases (~1/oxide thickness), as long as the oxide properties are comparable. The uptake rate increases again after the kinetic transition, due to the deterioration of the oxide scale. This deterioration can be enhanced by hydrogen, as it introduces additional defects inside the oxide layer. It is reported[86,87] that interstitial protons are bonded to lattice oxygen ions in zirconia. The term "substitutional hydroxide" is frequently used to refer to this defect[86]. The presence of hydrogen in zirconia influences the bonds of the neighbouring atoms, Zr and O.

The low thermal conductivity of zirconia induces an increase of the cladding temperature at the oxide/metal interface, which is intensifying, as the oxide scale is becoming thicker. Thermal gradients across the cladding wall will determine the redistribution of hydrogen (within the Zr substrate) towards the cooler outer surface. In these conditions, the formation of a hydride rim layer at the outer surface of the cladding tube has been observed[88].

Possible hydrogen species involved in the transport through the oxides scale could be hydrogen molecules, atoms or protons. The contribution of these species to the total hydrogen transport in zirconia is not well known, especially at low temperatures. One aim of this thesis is to improve the knowledge of hydrogen transport in zirconia at relevant temperatures for the nuclear industry.

The reduction of the hydrogen uptake in Zr-based alloys is crucial for a better performance of the structural materials inside the reactor, especially for higher burn up exposures. Various methods and procedures have been applied to improve the resistance to hydrogen absorption, including the use of inhibitors, coatings, thermal treatments and surface preparations. In **Paper I**, a promising method to reduce the hydrogen uptake rate in Zr-based oxide scale is presented. In **Paper IV**, positive and negative effects of hydrogen on the corrosion resistance of metals, alloys and semiconductors are analysed.

2.4 Second-phase particles: effects on corrosion

Chemical addition of Fe, Cr and Ni to pure Zr resulted in improved corrosion resistance in high temperature water and steam. The solubility of these elements in α-Zr is quite low (< 100 ppm)[6-9], and therefore they form precipitates like $Zr(Fe,Cr)_2$ and $Zr_2(Ni,Fe)$, known as second-phase particles (SPPs). The formation rate of protective oxides and also the thickness of these oxide layers were found to depend on the composition and initial size distribution of these SPPs. In BWR environments, nodular corrosion was observed when initially large size SPPs or agglomerated small size SPPs were present[23]. On the other hand, the dissolution of small-size SPPs in Zr-based materials during the in-reactor operation under high neutron flux in combination with hydrogen pick-up can enhance the deterioration of the oxide layer[11]. There is an optimum range for size distribution and composition of SPPs, which is correlated with the exposure conditions. Rudling and Wikmark[23] reported optimum size distributions for SPPs in the range of approximately 25-175 nm for BWR conditions. Optimum SPP Fe/Cr ratios of 0.6-1.2 and Fe/Ni ratios of 0.9-1.0 have also been found[23]. The distribution of Fe, Cr and Ni within the intermetallic phases affects the dissolution of this particles during irradiation[10]. Cr-containing particles were found to be less resistant than Ni-containing particles[11,23].

Abolhassani et al.[89] performed in situ studies of the oxidation of Zircaloy-4 at 700°C using environmental scanning electron microscopy (ESEM). The samples were also characterized with atomic force (AFM) and transmission electron microscopies (TEM). They found that after the uppermost precipitates start to oxidise, the surface oxide, above the respective precipitates, became depleted in Zr, showing a lens-type feature. This is due to an outward diffusion of Fe (and Cr) probably via grain boundaries, which will then be oxidised at the O/G interface. AFM revealed a granular morphology for the pretransition oxide and the presence of randomly distributed pores with non-uniform size and geometry[89]. In the vicinity of SPPs, cracks lying parallel to the interface were identified. The presence of the catalytically active SPPs at surfaces and interfaces can increase the effective activity of dissociated species like O^{n-}, OH^- and H^+. Two effects must be considered, i) the increased dissociation rate at the oxide/gas interface and ii) the induced space charge in the subsurface area. The un-oxidized SPPs, which can be found in the oxide layer up to approximately 1 μm away from the oxide/Zr(O) interface, can influence the electron and hydrogen transport across the oxide layer[23]. A short circuit pathway for these species via SPPs is operative as long as the un-oxidized SPPs are in contact with both, the environment and the metal substrate. Doping the zirconia lattice with lower valence and size cations, which diffuse away from the SPPs, will contract the zirconia lattice and will stabilize the tetragonal phase[90]. When the SPPs will start to be oxidized, additional stress is introduced due to the volume mismatch between the metallic SPPs and the newly oxidized SPPs (Pilling-Bedworth ratio > 1)[90]. The dissolution of the SPPs generates significant degradation of the oxide scale. Considerably higher oxidation rates and hydrogen uptake rates have been thus observed[23].

2.5 Effects of irradiation

In water-cooled nuclear reactors, the Zr-based structural materials are exposed in high temperature water/steam under irradiation conditions. Irradiation is produced by collisions with high energy neutrons, ions, photons and electrons[20]. The size, mass and energy of these species determine the extent of the deterioration. Irradiation induces changes in the exposed materials (metal/oxide scales) and in the exposure environment (water chemistry)[20].
It is well known that the corrosion of Zr-based materials is enhanced due to irradiation[9]. Changes in the microstructure of these alloys involve phase transition, dislocations, dissolution, reprecipitation and amorphisation[9,91]. The mechanical properties are seriously affected. Dissolution of the SPPs during in-reactor exposure is significantly accelerated[11]. The distribution of Fe, Cr and Ni within the intermetallic phases affects the dissolution of this particles during irradiation[10]. The Cr-containing SPPs were found to be more susceptible for dissolution than the Ni-containing SPPs[11,23]. Irradiation effects are rather different at low and high temperatures. Low temperature induced defects have more permanent character. A high dislocation density has been observed in Zircaloy-4 oxide scales formed in PWR conditions[41].

Irradiation of zirconia with low energy ions and neutrons generates increased abundance of vacancies and interstitials[20]. The formation of cavities or pores due to irradiation-induced defect association can occur under these conditions. Increased ionic and electronic conductivity is the direct result of the increased defect concentration and mobility in the oxide. The stability of the tetragonal phase is enhanced under irradiation conditions. Optical and thermal properties are also influenced by irradiation.

The water chemistry is significantly affected by radiation-induced radiolysis[9]. Active oxidizing radicals are produced during irradiation of water with high-energy electrons, protons or neutrons[3]. It is reported that the radiolysis of water is mainly controlled by the radiolysis near the metal surface or in small pores. Among the radiolysis products, hydrogen peroxide has a crucial effect on corrosion[3]. Deliberate hydrogen additions (a few wt ppm) to the coolant in the Light Water Reactors, LWRs, are aimed to reduce the negative effect of oxidizing radicals produced by water radiolysis. In BWRs, the noble metal chemical addition (NMCA) treatment is used to decrease the amount of dissolved oxygen species by catalysing the reaction between these species and the dissolved hydrogen (water production)[13]. By this method, the amount of dissolved hydrogen necessary to maintain a low content of oxygen radicals can be substantially reduced as well as the risk for intergranular stress corrosion cracking.

2.6 Naturally stable isotopes

In nature all elements exist in the form of isotopes. The isotopes of an element show similar chemical reactivity and differ just in mass having different number of neutrons (but the same number of protons)[92]. In our isotopic studies, the isotopes of ***H, O, C, Zr*** and ***Y*** have been used. In Table 2, the natural abundance of the above-mentioned isotopes is presented.

Table 2. Natural abundance,%, of ***H, O, C, Zr*** and ***Y*** stable isotopes (based on the ^{12}C standard) as well as their atomic number, Z, and weight[93]

Element	*Z*	*Isotope*	*Atomic weight, amu*	*Abundance, %*
Hydrogen	1	^{1}H	1.007	99.985
	1	^{2}H (D)	2.014	0.0115
	1	^{3}H (T)	3.016	not stable
Oxygen	8	^{16}O	15.9949	99.757
	8	^{17}O	16.999	0.038
	8	^{18}O	17.999	0.205
Carbon	6	^{12}C	12.00	98.9
	6	^{13}C	13.00	1.10
Zirconium	40	^{90}Zr	89.90	51.45
	40	^{91}Zr	90.90	11.27
	40	^{92}Zr	91.90	17.17
	40	^{94}Zr	93.90	17.33
	40	^{96}Zr	95.90	2.78
Yttrium	39	^{89}Y	88.90	100

Using the Gas Phase Analysis (GPA) technique, the isotopic composition of a gas mixture can be analyzed. Using other complementary isotope-sensitive techniques such as SIMS, the distribution of the isotopes in the reaction product (solid) can be investigated (all the above listed isotopes).

2.6.1 Isotopic effects

The substitution between isotopes results in effects generally termed as "isotope effects"[94].

The kinetic isotope effect appears mainly due to the difference in the mass of the exchanged isotopes (the vibrational frequency of an atom in a crystal lattice is proportional with $\frac{1}{\sqrt{M_{atom}}}$, where M_{atom} is the mass of the respective atom).

The strongest isotopic effect is found in the case of hydrogen, D having twice the mass of H.

2.7 Conclusions

A simplified view of the pretransition oxide film formation on a Zr-based alloy in oxygen/water/steam is shown in Figure 2.11:

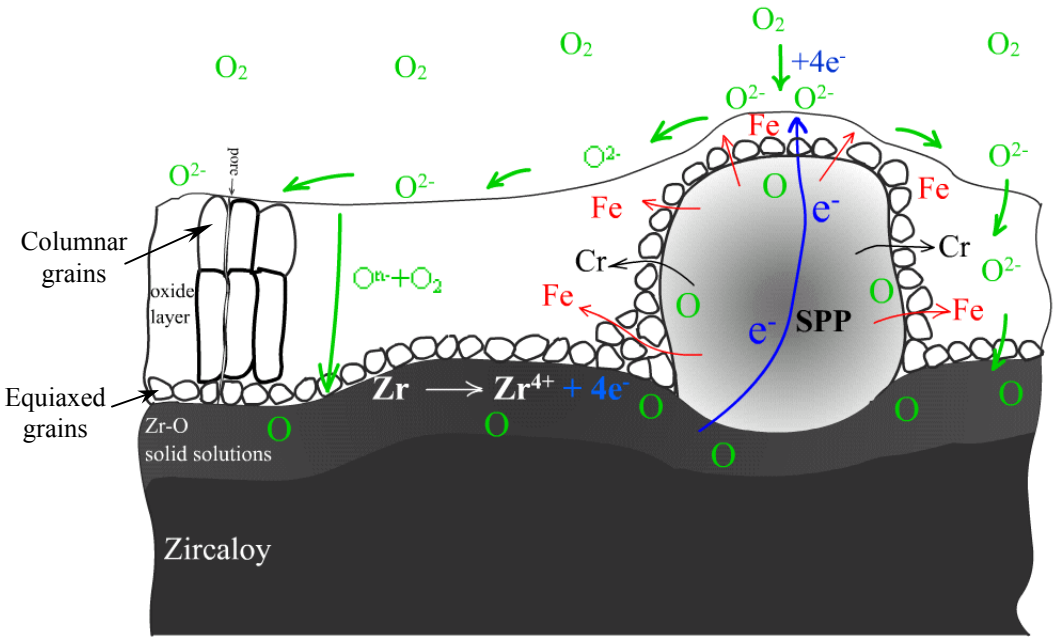

a.

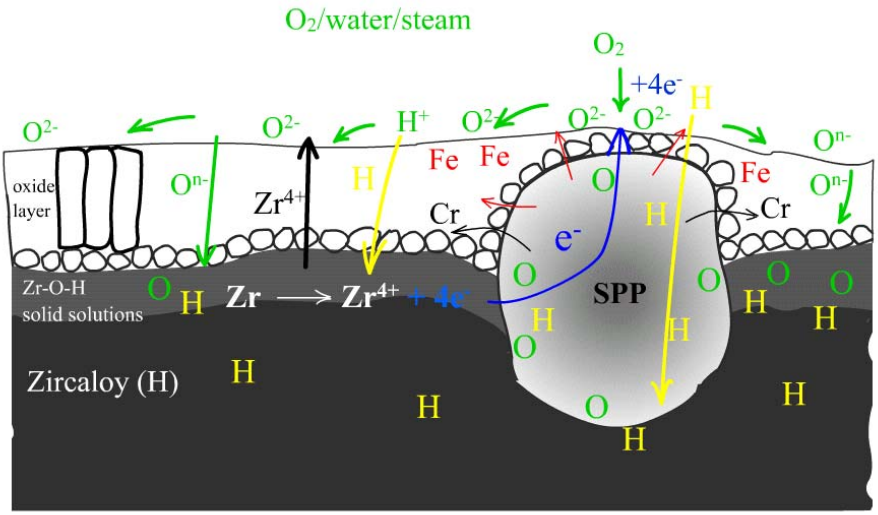

b.

Figure 2.11 Schematic view of the oxidation of a Zr-based alloy in the pretransition stage

a. oxidation in O_2 gas

b. balanced oxide growth with optimized inward oxygen and outward Zr^{4+} transport as a result of the presence of SPPs and a certain amount of hydrogen in the system (in the environment as water/steam or inside the oxide/metal substrate)

2.8 References

(1) G.P. Sabol in: Zirconium in the Nuclear Industry: 14th International Symposium, **2004**, Stockholm, Sweden, ASTM International, STP 1467, p.3.

(2) http://www.dpg-physik.de/static/fachlich/ake/vortragsammlung/03/06-Gelfort.pdf. **August 2006**.

(3) *IAEA-TECDOC-996, Viena* **1998**, p.27.

(4) K.L. Murty, I. C. *Progress in Nuclear Energy,* **2006**, *48*, p. 325.

(5) B. Cox, *Journal of Nuclear Materials,* **2005**, *Vol. 336*, p. 331.

(6) D. Setoyama, *Journal of Nuclear Materials,* **2005**, *Vol. 344*, p. 291.

(7) D. Arias; T. Palacios; C. Turillo, *Journal of Nuclear Materials* **1987**, *148*, p.227.

(8) P. Barberis; E. Ahlberg; N. Simic; D. Charquet; C. Lemaignan; G. Wikmark; M. Dahlbäck; M. Limbäck; P. Tängtström; B. Lehtinen in: Zirconium in the Nuclear Industry: 13th International Symposium, **2001**, Annecy, France, ASTM International, STP 1423, p. 33.

(9) C. Lemaignan in: Zirconium in the Nuclear Industry: 13th International Symposium, **2001**, Annecy, France, ASTM International, STP 1423, p. 20.

(10) P. Rudling; G. Wikmark, *Journal of Nuclear Materials* **1999**, *Vol. 265*, p. 44.

(11) P. Tägtström; M. Limbäck; M. Dahlbäck; T. Andersson ; H. Pettersson in: Zirconium in the nuclear industry: 13th International Symposium, **2001**, Annecy, France, ASTM International, STP 1423, p. 96.

(12) P.R. Roberge, *Handbook of Corrosion Engineering*; McGraw-Hill Companies Inc., **2000**.

(13) S. Hettiarachchi; R.L. Cowan; R.J. Law; T.P. Diaz, United States Patent 5719911, **1998**.

(14) J. Arborelius, et al. in: Zirconium in the Nuclear Industry: 14th International Symposium, **2004**, Stockholm, Sweden, ASTM International, STP 1467, p. 526.

(15) http://www.westinghousenuclear.com/pdf/NF_ES_Performance_Plus_Fuel.pdf. **May 2006**.

(16) P. Kofstad, *High Temperature Corrosion*; Elsevier Applied Science: London and New York, **1988**.

(17) A. P. Zhilyaev; J. Szpunar, *Journal of Nuclear Materials* **1999**, *264*, 327.

(18) M.B. Elmoselhi, *Journal of Alloys and Compounds* **1995**, *231*, p.716.

(19) M. Tupin et al., *Materials Science Forum* **2004**, *461-464*, p.13.

(20) C. Gibert, Raport CEA-R-5848, **1999**.

(21) A.Yilmazbayhan; E. Breval; A.T. Motta; R.J. Comstock, *Journal of Nuclear Materials* **2006**, *349*, p.265.

(22) B. Cox, *Journal of Nuclear Materials* **1968**, *25*, 310.

(23) P. Rudling; G. Wikmark, *Journal of Nuclear Materials* **1999**, *265*, 44.

(24) H.D. Wiemhöfer, *Solid State Ionics* **1995**, *75*, 167.

(25) N. Mizutani; J. Nowotny, *Journal of Materials Synthesis and Processing* **1998**, *6*, p.401.

(26) S. A. Raspopov et al., *Journal of Chemical Society Faraday Transactions* **1997**, *93*, p.2113.

(27) X. Iltis et al., *Journal of Nuclear Materials,* **1993**, *209*, p.180.

(28) X. Iltis, B. Stauder, H. Michel, C. Frantz. *Surface Coatings Techol.* **1993**, *60*, p.405.

(29) *Gas Sensors. Principles, operation and developments,* G. Sberveglieri (Ed.), Kluwer Academic Publishers, **1992**.

(30) J.P. Goff; W. Hayes; S. Hull; M.T. Hutchings; K.N. Clausen, *Physical Review B* **1999**, *59*, p. 14202.

(31) J.W. Fergus, *Journal of Materials Science* ***2003***, *38*, p.4259.

(32) R.J. Stafford et al., *Solid State Ionics* **1989**, *37*, p.67.

(33) J.-C. M'Peko et al., *Applied Surface Physics Letters* **2003**, *83*, p.737.

(34) P. Li et al., *Journal of the American Ceramic Society* **1994**, *77*, p. 118.

(35) K. Dae-Joon et al., *Journal of the American Ceramic Society* **1997**, *80*, p. 1453.

(36) S. Abolhassani; M. Dadras; M. Leboeuf; D. Gavillet, *Journal of Nuclear Materials* **2003**, *321*, p. 70.

(37) G.A. Eloff et al., *Journal of Nuclear Materials,* **1993**, *199*, p. 285.

(38) P. Kofstad, *Oxidation of Metals* **1995**, *44*, p. 3.

(39) K. R. Lawless, *Rep. Prog. Phys.* **1974**, *37*, p. 231.

(40) A. Madeyski; D.J. Poulton; W.W. Smeltzer, *Acta Metalurgica* **1969**, *17*, 579.

(41) S. Abolhassani et al. in: Zirconium in the Nuclear Industry: 14th International Symposium, **2004**, Stockholm, Sweden, ASTM International, STP 1467, p.467.

(42) K. Otsuka et al., *Applied Physics Letters* **2003**, *82*, 877.

(43) P. Kountouros; G. Petzow in: *Science and Technology of Zirconia V*; Technomic Publishing Co, Lancaster, Basel, S.P.S. Badwal, M.J. Bannister, R.H.J. Hannink, (Eds.), **1993**, p 34.

(44) A. Yilmazbayhan et al., *Journal of Nuclear Materials* **2004**, *324*, p.6.

(45) H. Anada et al. in: Zirconium in the Nuclear Industry: 11th International Symposium, **1995**, Garmisch-Partenkirchen, Germany, ASTM International, STP1295, p. 74.

(46) D. Pęcheur; J. Godlewski; P. Billot; J. Thomazet in: Zirconium in the Nuclear Industry: 11th International Symposium, **1995**, Garmisch-Partenkirchen, Germany, ASTM International, STP1295, p. 94.

(47) V.V. Kharton et al., *Journal of Solid State Electrochem.* **1999**, *3*, p. 61.

(48) M. de Ridder et al., *Solid State Ionics* **2003**, *158*, p. 67.

(49) P.S. Manning; J.D. Sirman; R.A. De Souza; J.A. Kilner, *Solid State Ionics* **1997**, *100*, p.1.

(50) N. Sakai et al., *Journal of Alloys and Compounds* **2006**, *408-412*, p. 503.

(51) N. Ramasubramanian; P. Billot; S. Yagnik in: Zirconium in the Nuclear Industry: 13th International Symposium, **2001**, France, ASTM International, STP1423, p. 222.

(52) A. Lyapin; L.P.H. Jeurgens; E.J. Mittemeijer, *Acta Materialia* **2005**, *53*, p. 2925.

(53) C. Zhang; P.R. Norton, *Journal of Nuclear Materials* **2002**, *300*, p. 7.

(54) I.G. Ritchie; A. Atrens, *Journal of Nuclear Materials* **1974**, *50*, p. 247.

(55) P.A. Perkins, *Journal of Nuclear Materials* **1977**, *68*, p. 148.

(56) B. Cox; J.P. Pemsler, *Journal of Nuclear Materials* **1968**, *28*, p. 73.

(57) E.A. Gulbransen; K.F. Andrew, *Journal of Metals* **1957**, p. 349.

(58) M. Kilo et al., *Defect and Diffusion Forums* **2001**, *194-199*, p. 1039.

(59) P.J. Harrop, *Journal of Materials Science* **1968**, *3*, p. 206.

(60) M. Kilo et al., *The Journal of Chemical Physics* **2004**, *121*, p. 5482.

(61) M. Kilo et al., *Journal of Applied Physics* **2003**, *94*, p. 7547.

(62) G. Hultquist; B. Tveten; E. Hörnlund; M. Limbäck; R. Haugsrud, *Oxidation of Metals* **2001**, *56*, p. 313.

(63) G. Hultquist; G. I. Sproule; S. Moisa; M.J. Graham; U. Södervall, *Journal of Electrochemical Society* **2003**, *150*, p. G617.

(64) V.V. Fedorov et al., *Defect and Diffusion Forums* **2001**, *194-199*, p. 1105.

(65) G.Z. Cao, *Journal of Applied Electrochemistry* **1994**, *24*, p. 1222.

(66) T. Nishizaki et al., *Journal of Alloys and Compounds* **2002**, *330-332*, p.307.

(67) J.H. Eriksen; K. Hauffe, *Zeitschrift für Physikalische Chemie Neue Folge* **1968**, *59*, p.332.

(68) M.B. Elmoselhi, *Journal of Alloys and Compounds* **1995**, *231*, p.716.

(69) T. Laursen et al., *Journal of Nuclear Materials* **1994**, *209*, p. 52.

(70) A. Sawatzky. *Journal of Nuclear Materials* **1960**, *2*, p. 62.

(71) N. Dupin et al., *Journal of Nuclear Materials* **1999**, *275*, p. 287.

(72) J.J. Kearns, *Journal of Nuclear Materials* **1967**, *22*, p. 292.

(73) S. Yamanaka; M. Miyake; M. Katsura, *Journal of Nuclear Materials* **1997**, *247*, p. 315.

(74) D. Setoyama et al., *Journal of Nuclear Materials* **2005**, *344*, p. 291.

(75) I. Takagi et al., *Journal of Nuclear Science and Technology* **2002**, *39*, p. 71.

(76) M. Miyake et al., *Journal of Nuclear Materials* **1999**, *270*, p. 233.

(77) C. -S. Zhang; B. Li; P.R. Norton, *Journal of Alloys and Compounds* **1995**, *231*, p. 354.

(78) D. Setoyama; S. Yamanaka, *Journal of Alloys and Compounds* **2004**, *370*, p. 144.

(79) B.H. Lim et al., *Journal of Nuclear Materials* **2003**, *312*, p. 134.

(80) D. Khatamian; F.D. Manchester, *Journal of Nuclear Materials* **1989**, *166*, p. 300.

(81) N.S. McIntyre et al., *Journal of Vacuum Science and Technology A.* **1991**, *9*, p. 1402.

(82) T. Smith, *Journal of Nuclear Materials* **1966**, *18*, p. 323.

(83) D.J. Mitchell, *Journal of Vacuum Science and Technology A.* **1984**, *2*, p. 780.

(84) G. Leličvre; C. Tessier; X. Iltis; B. Berthier; F. Lefebvre, *Journal of Alloys and Compounds* **1998**, *268*, p. 308.

(85) C. Andrieu; S. Ravel; G. Ducros; C. Lemaignan, *Journal of Nuclear Materials* **2005**, *347*, p. 12.

(86) T. Norby in: *Zirconia'88 - Advances in Zirconia Science and Technology*; S. Meriani, C. Palmonari (Eds.); Elsevier Applied Science: London and New York, **1988**; p 209.

(87) T. Norby in: *Selected Topics in High Temperature Chemistry. Defect Chemistry of Solids*; Elsevier Science Publishers B.V., Ø. Johannesen, A.G. Andersen (Eds.) **1989**, p. 101.

(88) R.S. Daum; S. Majumdar; D.W. Bates; A.T. Motta; D.A. Koss; M.C. Billone, in: Zirconium in the Nuclear Industry: 13th International Symposium, **2001**, Annecy, France, ASTM International, STP 1423, p. 702.

(89) S. Abolhassani; M. Dadras; M. Leboeuf; D. Gavillet, *Journal of Nuclear Materials* **2003**, *321*, p. 70.

(90) J.H. Baek; Y.H. Jeong, *Journal of Nuclear Materials* **2002**, *304*, p. 107.

(91) S. Doriot et al. in: Zirconium in the nuclear industry: 14th International Symposium, **2004**, Stockholm, Sweden, ASTM International, STP1295, p.175.

(92) M.E. Wieser; W.A Brand, *Encyclopedia of Spectroscopy and Spectrometry*; Academic Press, **2000**.

(93) *CRC Handbook of Chemistry and Physics, chapter 6*, 80 edition; D. Linde (Ed.), CRC Press LLC, **1999-2000**.

(94) J. Gross, *Mass Spectrometry*; Springer, **2004**.

Chapter 3

Experimental techniques

with some experimental results

3.1 Gas Phase Analysis (GPA)

GPA is a useful tool for characterization of complex processes, identification and characterization of reaction mechanisms and transport modes (transport in molecular and/or dissociated form) during the interaction between solids and below. In-situ information is obtained by combining manometric and mass spectrometric data. A complementary isotopic sensitive technique such as Secondary Ion Mass Spectroscopy (SIMS) can be used to characterize the reaction products.

The GPA equipment, presented in Figure 3.1 consists of:

- A "virtually closed reaction" chamber
- A gas handling system for the introduction of the isotopic gas mixtures and a pressure gauge for total pressure measurements
- A mass spectrometer equipped with a quadrupole analyser, placed in an UHV chamber (which is pumped with an ion pump).
- A tube furnace, which can be used up to 1200°C.

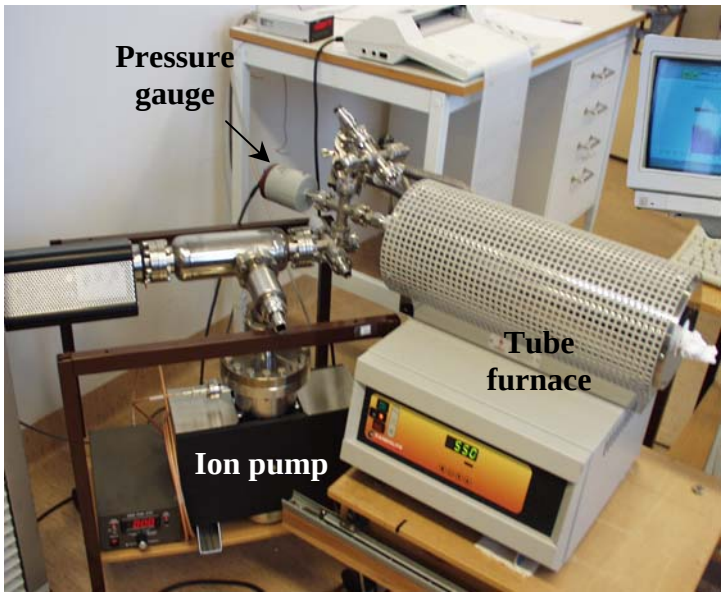

$^{18,18}O_2$ –containing tube

Figure 3.1 Gas Phase Analysis equipment

The GPA equipment can be used to study in-situ solid-gas interactions by:

- *Exposure of solids to isotopic gas mixtures*
- *Outgassing of solids (vacuum annealing)*
- *Permeation of gases through solid membranes*

A detailed description of these in-situ investigations can be found in **Paper V**. General aspects related to GPA are described as follows.

3.1.1 Exposure of solids to isotopic gas mixtures

During the exposure of a solid to isotopic gas mixtures, the composition of the gas phase can be continuously monitored using the mass spectrometer (MS) via a leak valve (negligible gas consumption).

If we consider an oxide, Me_xO_y, as a starting material which is exposed to different oxygen isotopic gas mixtures, ($^{16,16}O_2$+ $^{18,18}O_2$), the following situations can be identified:

a. Isotopic exchange takes place between the oxygen molecules from the gas phase ($O_2 \Leftrightarrow O_2$) as a result of the catalytic activity of the oxide surface (Figure 3.2a)

b. Isotopic exchange takes place between the oxygen molecules from the gas phase and lattice oxygen ($O_2 \Leftrightarrow Me_x{}^{16}O_y$) due to thermodynamic equilibration between the oxide and the gas phase (Figure 3.2b)

As a result of the isotopic exchange, the mixed oxygen molecules $^{16,18}O_2$ will form in the gas phase. Schematics of the time evolution of $^{16,18}O_2$ abundance in the gas phase as well as the abundance of the ^{16}O and ^{18}O (initial gas composition 51% ^{16}O and 49%^{18}O) are also shown in the figure.

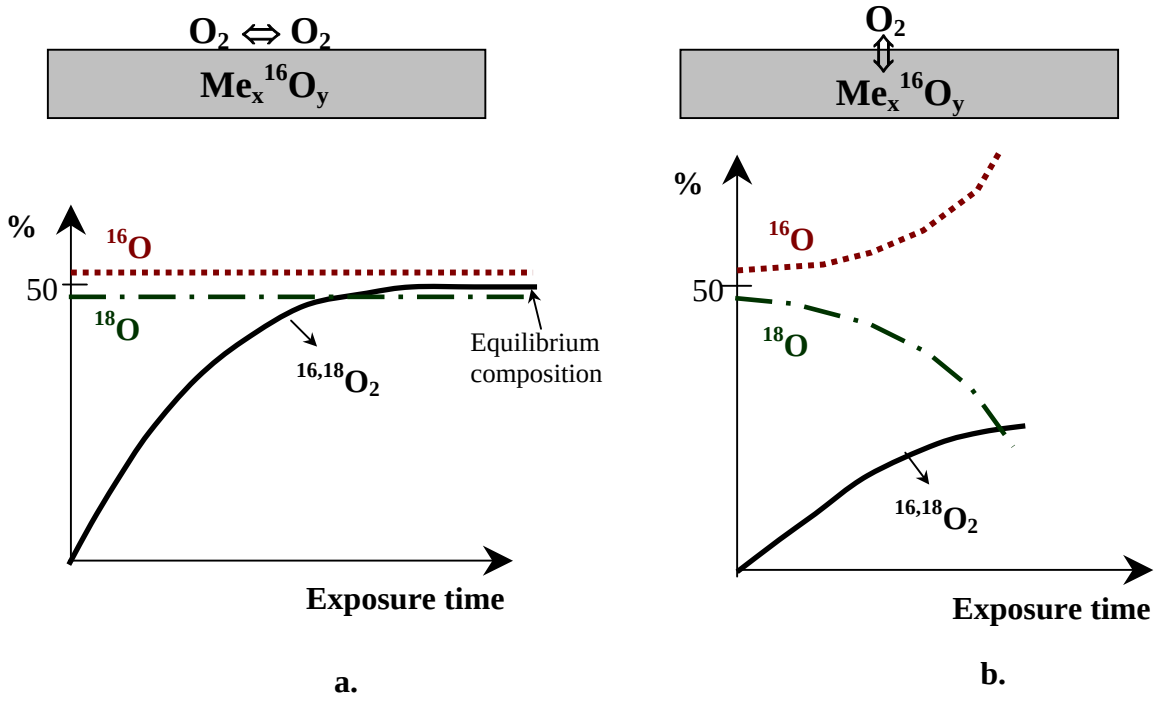

Figure 3.2 Schematics of oxygen isotopic exchange upon exposure of an oxide, $Me_x{}^{16}O_y$, to ^{18}O-containing oxygen gas (49%^{18}O). a. $O_2 \Leftrightarrow O_2$ exchange and b. $O_2 \Leftrightarrow Me_x{}^{16}O_y$ exchange

In Figure 3.2 the exchange rate is proportional to the initial formation rate of the mixed molecules in the gas phase. The increase of the ^{16}O content, %, in the gas phase is a

consequence of the $O_2 \Leftrightarrow Me_x{}^{16}O_y$ exchange as seen in Fig. 3.2b. For simplicity the statistical equilibrium is illustrated just in Fig. 3.2a.

In **Paper VI**, oxygen exchange on $Zr^{16}O_2$ at temperatures between 400 and 900°C is investigated. Hörnlund[1] recently published a detailed study of oxygen dissociation on solid surfaces at high temperatures using the GPA technique.

If we consider a metal, Me, as a starting material, the kinetics and mechanisms of gas uptake in the metal can be investigated using isotopic gas mixtures. The gas uptake is proportional with the pressure decrease in the reaction chamber and can be quantified. The mechanisms involved in the transport process may be evaluated using for example SIMS depth profiling.

It is important to point out that during the same experiment, additional information can be obtained by combining manometric measurements with isotopic information.

In **Paper I**, hydrogen uptake in a preoxidized Zircaloy-2 (2 μm oxide thickness) is analysed at 300°C as well as hydrogen dissociation. The results show that the hydrogen dissociation rate on preoxidized Zircaloy-2 exceeds the hydrogen uptake rate at 300°C. This suggests that dissociated hydrogen species are involved in the transport at this temperature. In addition, the dissociation of CO on different materials upon exposure to $^{12}C^{16}O+^{13}C^{18}O$ gas mixtures has been investigated in the temperature range of 400-900°C (**Paper I**).

In **Paper II**, two-stage oxidations have been used to study the influence of Pt and D on the oxidation of Zr.

3.1.2 Outgassing of solids (vacuum annealing)

Gas release can occur during the heating of a sample in vacuum. Identification and quantification of the released gas is performed using a mass spectrometer equipped with a quadrupole analyser. The sample is placed in the reaction chamber and the released gas is continuously removed with an ion pump via a fully opened leak valve. MS analyses the composition of the gases released by outgassing and the computer graphically reproduces the partial pressure of the gas constituents. By this method, the hydrogen content in a material can be quantified (**Paper II**, hydrogen outgassing from Zr).

In **Paper III** (and **Paper V**), a model is proposed for estimation of gas transport in porous oxides based on quantitative outgassing.

A combination of uptake-release type of measurements, using isotopic gas mixtures is described in **Paper VI** and exemplified with measurements of oxygen transport in zirconia.

3.1.3 Permeation of gases through solid membranes

Oxide membranes can be self-supporting or constitute a scale on a metal substrate. The driving force for the transport of species like oxygen and hydrogen through oxide membranes is the activity gradient across the membrane (oxide scale). A schematic representation of a simple membrane model[2-4] for oxidation of a metal substrate by inward oxygen transport is presented in Figure 3.3. The figure shows the effect of Pt on the oxygen transport through the oxide scale during oxidation[2-4].

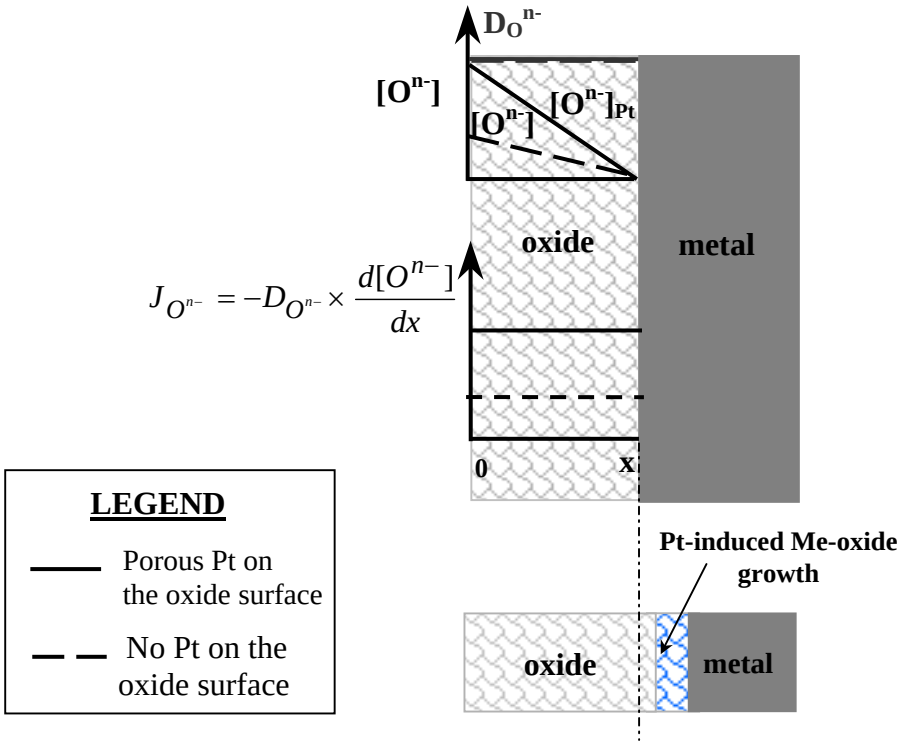

Figure 3.3 Membrane model[2-4] for oxygen transport in an oxide scale that grows by inward oxygen transport, showing the effect of Pt on the oxide growth.

$\mathbf{D_O^{n-}}$ represents the diffusivity of oxygen ions in the oxide scale,

$\frac{d[O^{n-}]}{dx}$ = oxygen activity gradient across the membrane ($[O^{n-}]_{Pt}$ for the Pt coated sample),

x = membrane thickness,

$J_{O^{n-}}$ = total oxygen flux.

Figure 3.3 shows that the flux of dissociated oxygen species (O^{n-}, n= 0, 2) is increased due to Pt addition at the oxide/gas interface. The increased flux results in increased oxide growth at the metal/oxide interface. The validity of this simple membrane model relies on a number of conditions:

a. A perfect gas tight oxide membrane
b. Fast reactions at the metal/oxide interface; virtually zero oxygen activity at this interface
c. Oxide growth exclusively at the metal/oxide interface.

Oxygen diffusivity, $\mathbf{D_O^{n-}}$, in the oxide is not influenced by Pt.

$\frac{d[O^{n-}]}{dx}$ increases due to Pt addition at the oxide/gas interface, resulting in Pt-induced enhanced oxidation.

Perfectly gas-tight oxide scales are generally desired but practically the molecular transport must also be considered. Investigation of the total oxygen transport through oxide membranes/scales can be performed using isotopic gas mixtures in combination with mass spectrometry.

After the oxygen gas is introduced at the high-pressure side of a membrane, the flux of the permeated gas at the low-pressure side increases until the rate becomes constant (steady state flux).

The steady state flux, F, can be used to calculate oxygen permeability, K, as shown below[5]:

$$K = \frac{F \times L}{A \times P}, \qquad [\mu mol\ cm^{-1}\ s^{-1}\ atm^{-1}]$$

where,

F- total oxygen flux, μmol s^{-1}

L - the membrane thickness, cm

A - surface area of the membrane, cm^2

P – pressure at the feed side (HP side), atm.

P can be approximated with the pressure at the high-pressure side (UHV at the low-pressure side).

Investigations of the transport properties of membranes have been performed using isotopic gas mixtures as well as inert gases. The gas composition at the high-pressure and the low-pressure sides of the membrane are monitored continuously with mass spectrometers and the flux of the permeated gas is evaluated.

The mass spectrometer measures the partial pressure of the permeated gas components. To convert the obtained data into flux units, μmol cm^{-2} s^{-1}, the MS needs to be calibrated. **Paper V** describes in detail the setup in use as well as the calibration procedures.

In **Paper VI**, permeation of labeled oxygen in zirconia was used to identify to what extent molecular and dissociated oxygen species are transported in zirconia at temperatures between 400 and 900°C.

3.2 Secondary Ion Mass Spectrometry

SIMS analyses were performed with a Cameca IMS-6f apparatus, 10 keV, 50-200 nA primary beam of Cs^+ ions, which was rastered over 200x200 μm^2, where ions where detected from a centred area with a diameter of 70 μm.

Oxidation mechanisms can be investigated by using two-stage oxidation, first in $^{16,16}O_2$ followed by the exposure to ^{18}O-enriched oxygen gas, and a subsequent SIMS depth profiling. The oxide growth mode can be retrieved as illustrated in Figure 3.4.

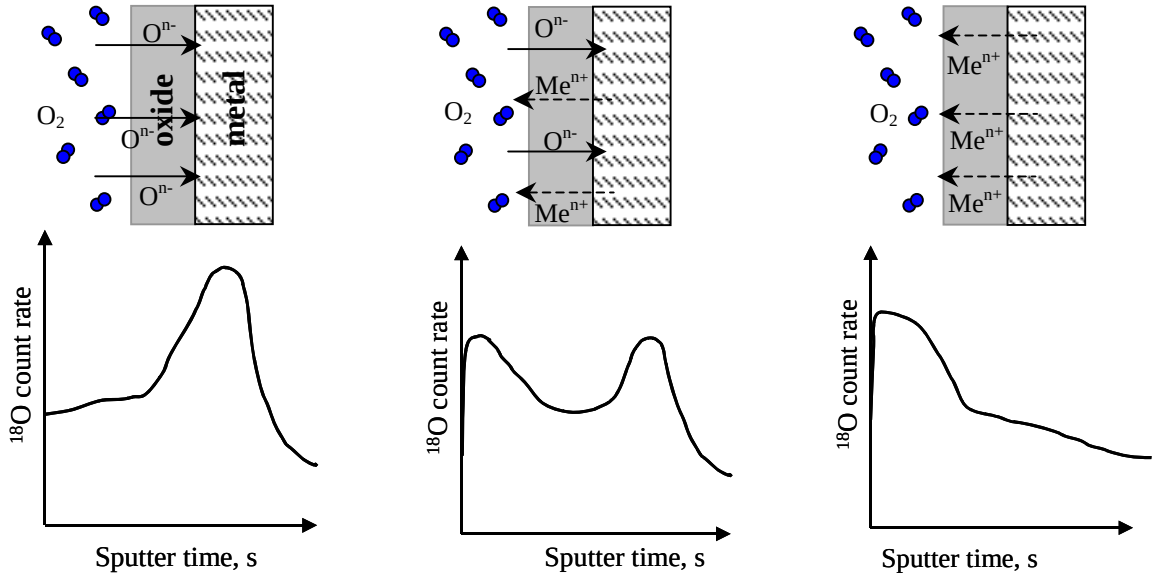

Figure 3.4 Evaluation of the mechanisms of oxide growth by ^{18}O SIMS depth profiling

The exchange with the lattice has to be considered when profiles like b. and c. (Figure 3.4) are obtained. When the exchange rate is negligible in comparison to the oxidation rate, it can be concluded that the mechanism of oxide growth for case b. is a balanced transport and for case c. mainly governed by outward metal transport.

The oxide thickness can be calculated based on the sputter time when the ^{90}Zr ion count rate has decreased to half of its maximum value.

SIMS depth profiles of $^{90}Zr^{18}O$, and $^{90}Zr^{16}O$ ions were used in addition to ^{18}O and ^{16}O profiles to investigate the oxide layer formation on a Zr surface (**Paper II**).

For an Y-stabilized ZrO_2 sample the preferential transport of oxygen via Y or Zr can be evaluated by analysing an ^{18}O-annealed Y-stabilized $Zr^{16}O_2$ sample with SIMS. A comparison of $Y^{18}O/Y^{16}O$, $Zr^{18}O/Zr^{16}O$ and $^{18}O/^{16}O$ ratios revealed that oxygen is transported anisotropically in the material. A high $Y^{18}O/Y^{16}O$ ratio compared to $Zr^{18}O/Zr^{16}O$ ratio suggests that oxygen exchange preferentially takes place with oxygen bonded to Y.

In **Paper II**, samples of 99.94% Zr-metal were partly coated with Pt and subsequently oxidized at 400°C in normal ^{16}O oxygen followed by ^{18}O-enriched oxygen. Oxidations were performed in a closed reaction chamber connected with a mass spectrometer. Oxygen uptake as well as oxygen dissociation were measured during exposure. From the SIMS-depth profiles of the formed oxide, the thickness of the oxide scale was determined at different positions on the samples. An analysis of the in-depth distribution of ^{18}O was performed, providing information on the oxide growth mode. The results are illustrated in the following ^{18}O-SIMS map (Fig. 3.5).

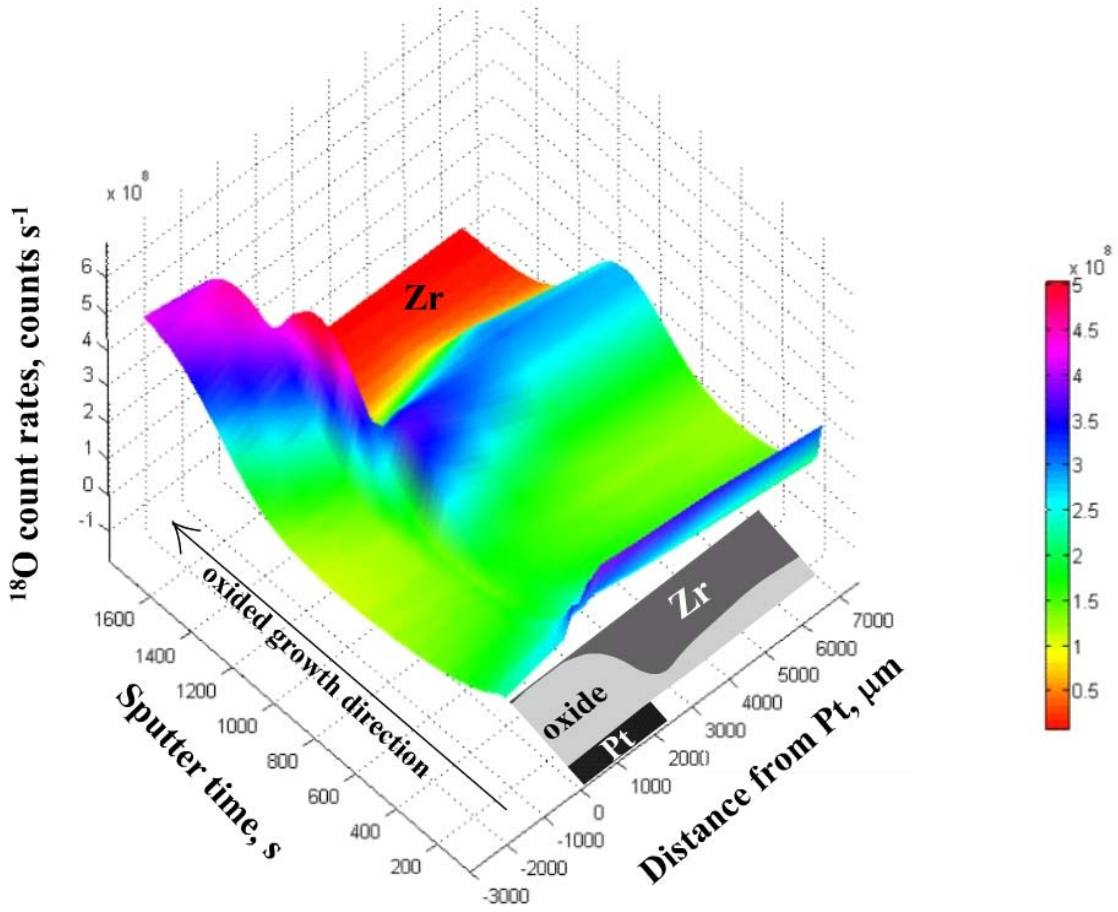

Figure 3.5 ^{18}O-SIMS map of a Zr sample partly coated with porous Pt and oxidized in two stages: first in normal ^{16}O oxygen followed by ^{18}O-enriched oxygen at 400°C

The oxide is growing mainly by inward oxygen transport (^{18}O was used in the second stage of oxidation and in the oxide ^{18}O is found mainly near the oxide/metal interface). SIMS profiles obtained at different distances from the Pt interface revealed a mm-ranged oxygen ion/atom spill-over effect. In the area with Pt particles, enhanced oxidation was observed, which resulted in thicker oxide scales. Another, even more interesting result was a local minimum in the oxide thickness adjacent to the area with Pt particles. An advantage of the SIMS technique is the capability of detecting hydrogen-containing species. Deuterium depth profiles provide valuable

information on the mechanism of hydrogen uptake. ^{18}OD SIMS profiles were considered to elucidate the possible connection between hydrogen and oxygen diffusion (**Paper II**).

3.3 X-Ray Photoelectron Spectroscopy

XPS analyses were performed with a Kratos AXIS HS spectrometer using a monochromatic Al Kα X-ray source (1486.6 eV). The area of analysis was approximately 0.4 mm^2.

The method is based on the photoelectric effect and an information depth of a few nm is obtained. Upon exposure of a sample to photons with relatively high incident energy, electrons from the inner shell of the atoms are released. The energy of these photoelectrons can be expressed as:

$$E_{kin} = h\nu - E_B - \Phi$$

where hν is the X-ray incoming energy, E_B is the binding energy of the electron and Φ is the work function of the material. The kinetic energy of the electron depends on the incident photon energy, but the binding energy is a physicochemical constant. Therefore, XPS can be used to identify which elements are present at the outermost surface of a sample and also to characterize the nature of the chemical bonds, which connects these atoms.

3.4 Scanning Electron Microscopy

SEM uses electrons to form the image of the surface of a sample. When the incoming beam of electrons hits the surface, photons, secondary and backscattered electrons are ejected from the sample. The ejected electrons are used in SEM to obtain high-resolution images of the topography or morphology of the surface. FEG-SEM analysis were performed with a Leo 1530 Field Emission Scanning Electron Microscope equipped with a GEMINI field emission column.

3.5 References

1. E. Hörnlund, Studies of dissociation of diatomic molecules with isotope spectroscopy. *Applied Surface Science* **2002**, *199*, p.195-210.
2. G. Hultquist, G.I. Sproule, S. Moisa, M.J. Graham, U. Södervall, *J. Electrochem Soc.* **2003**, 150, p. G617.
3. G. Hultquist, E. Hörnlund, C. Anghel and Q. Dong. in *Proceedings of 146th ISIJ Meeting,* Sapporo, Japan, **2003**.
4. C. Anghel, Q. Dong and G. Hultquist, Proceedings of the *13th Scandinavian Corrosion Congress, NKM 13,* Reykjavik, Iceland, 18-20 April, **2004**.
5. J.E. Shelby, *Handbook of gas diffusion in solids and melts* (ASM International, **1996**).

Chapter 4

Summary of appended papers

4.1 Paper I

Gas phase analysis of CO interactions with solid surfaces at high temperatures

In **Paper I,** the deactivation of a surface related to adsorption and dissociation of molecules has been examined and related to problems, which are common in industrial applications.
Using the GPA technique, the dissociation of hydrogen on preoxidized Zr and of carbon monoxide on oxidized Cr have been investigated. Carbon monoxide is well known for its poisoning effect on different catalysts.
Dissociation rates of carbon monoxide on various materials exposed to 20 mbar CO at different temperatures have been studied. High dissociation rates have been measured on materials such as pure Cr, Ni, Fe and stainless steel SS 304. It is interesting to note that these materials often suffer from high carbon uptake in CO containing atmospheres, a negative consequence of the high CO dissociation rates. On the other hand, relatively low dissociation rates were found on Zr, Cu, Al, Cu-8Al alloy, and Pt. CO adsorption on the surface of these materials can have a positive effect. Carbon monoxide is identified as an effective site blocker for hydrogen adsorption and dissociation on preoxidized Zircaloy-2 ($Zr2_{ox}$) at temperatures around 400°C. The uptake rate of hydrogen was substantially lowered (approximately 40 times) when 2 mbar carbon monoxide was added to the gas phase. No influence of nitrogen gas on the hydrogen uptake by Zircaloy-2 at 400°C was observed.

In CO exposure to Cr_2O_3, the influence of H_2O on the CO dissociation rate was investigated at 600°C. A decrease in the CO dissociation rate was observed as a result of water addition to the CO gas, which can be interpreted as a blocking effect of water on the surface. Upon a subsequent removal of water from the gas phase, the CO dissociation rate increased again. The results suggest that the surface activity for carbon monoxide dissociation should be a key factor for carbon uptake in certain applications and can be reduced by adsorbed water.

Based on the results of the present work, the following rating for the tendency of adsorption on $Zr2_{ox}$ and Cr_2O_3 at temperatures in the range 400-600°C has been made: $N_2 < H_2 < CO < H_2O$.

4.2 Paper II

Influence of Pt, Fe/Ni/Cr–containing intermetallics and deuterium on the oxidation of Zr-based materials

In **Paper II**, the transport of oxygen and hydrogen through the growing zirconia layer in the oxidation of Zr-based materials in O_2 at 400°C and in water vapour at 370°C was investigated using GPA and SIMS.

The paper is divided in three sections.

1. Oxygen dissociation on Zr-based materials and on Pt
2. Influence of Pt and deuterium on the oxidation of Zr in O_2 at 400°C
3. Oxidation of Zr-based tubes in water at 370°C

1. Oxygen dissociation on Zr-based materials and Pt

The results show that the oxygen dissociation efficiency at 400°C, decreases in the order:

$$Pt > Zr_2Fe > Zr_2Ni > ZrCr_2 \geq Zircaloy\text{-}2$$

It is important to note that the dissociation rate of O_2 on preoxidized Zr_2Fe is about 10^3 times higher compared to preoxidized Zircaloy-2 at 400°C.

2. Influence of Pt and deuterium on the oxidation of Zr in O_2 at 400°C

Two 1.8 cm^2 Zr plates (99.9% metal basis excl. Hf) were used in this study. One sample was charged from gas phase with deuterium to 600 wtppm D. Both samples were then partly coated with 200Å porous Pt. The samples were oxidized at 400°C in two stages, first in $^{16,16}O_2$ then in ^{18}O-enriched oxygen gas for totally 12 hours. After oxidation, the samples were characterized with SIMS, XPS, SEM and optical microscopy.

The following main conclusions were drawn:

- For both samples, an enhanced oxidation takes place in the area with Pt particles
- A spillover of the dissociated oxygen species from the area with Pt particles is identified with mm-range effect
- The overall oxidation rate (oxide thickness) is lower for the D-charged sample
- Outward diffusion of D is suppressed in the area with Pt particles
- The formation of “substitutional hydroxides” at the oxide/metal interface is proposed as a mechanism for oxide deterioration. Hydrogen may also induce Zr diffusion in the oxide, resulting in new oxide formation with fewer defects. If the hydrogen content is high the dissolution rate may become higher than the healing capacity of the oxide and deterioration may occur.

3. Oxidation of Zr-based tubes in water at 370℃

Two Ar-filled Zr-based tubes (1 m long) were exposed to 22 mbar water vapour at 370°C for 305 and 630 minutes. The oxide thickness and the hydrogen content were measured at different positions from the water inlet using SIMS depth profiles.
A gradient in the hydrogen content inside these Zr-based tubes resulted in a non-homogeneous oxide thickness. The results show that the hydrogen content in the substrate influences the oxide scale growth.

Conclusions

A balance between inward oxygen and outward metal diffusion has been previously proposed as an important condition for obtaining oxides of high protective ability e.g. zirconium oxide.

- The *inward flux of oxygen ions* can be promoted by ensuring a high catalytic activity for oxygen dissociation on the Zr surface (by Pt coating or increasing the fraction of the second-phase particles at the surface). It is proposed that Fe-containing second-phase particles act as oxygen dissociating elements in an analogue way as Pt.
- The *outward flux of Zr cations*, on the other hand, can be promoted by introducing hydrogen in the oxide/metal. It is suggested that this phenomenon is beneficial for healing defects such as pores and microcracks, which are mainly formed in the zirconium oxide scale during oxidation caused by the inward oxygen diffusion.

Hence, a proper choice of second-phase particles composition and size distribution can be beneficial for reducing the negative effect of hydrogen uptake.

4.3 Paper III

Gas-tight oxides - Reality or just a Hope

Paper III presents a novel and relatively straightforward method to characterize the gas release from an oxide previously equilibrated in a controlled atmosphere. A desorption experiment, involving a mass spectrometer placed in ultra high vacuum, can be used to determine the diffusivity and the amount of gas released with aid of a mathematical model. The method is validated in measurements of diffusivity and solubility of He in quartz and applied by characterizing two Zr-oxides and one Fe oxide (air-equilibrated). From the outgassed amounts of water and nitrogen the H_2O/N_2 molar ratio can be used to estimate an effective pore size in oxides.

Results

It was found that:

- the diffusivity of N_2 at 80°C in pretransition Zr-based oxides is in order of 10^{-13} cm^2 s^{-1}
- the diffusivity of N_2 at 20°C in a 0.3mm thick Fe-oxide is in the order of 10^{-9} cm^2 s^{-1}.
- The effective pore diameters in pretransition oxide scales on Zircaloy-2 (ϕ =1-10 nm) are considerably smaller that for the Fe-oxide (ϕ = 100-1000nm).
- Significant transport of molecular species was identified in pretransition oxides on Zircaloy-2 and in Fe-oxide, which means that at the measurements conditions **these oxides are not gas-tight.**

4.4 Paper IV

Effects of hydrogen on the corrosion resistance of metallic materials and semiconductors

In **Paper IV**, positive and negative effects of hydrogen on the corrosion behaviour of metals, alloys and semiconductors are identified.

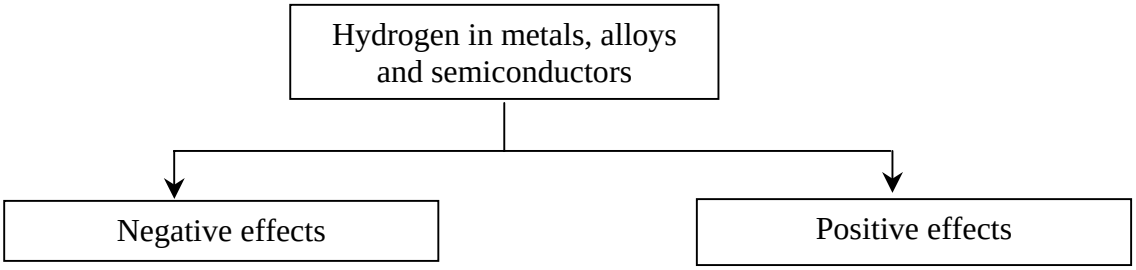

- Formation of brittle hydrides
- Decreased pitting corrosion resistance of Cr, stainless steel grades SS 304 and SS 310 in aqueous solutions
- Increased anodic dissolution rate
- Higher oxidation rate in H-containing Fe and Cr (loss of adherence)
- Enhances the oxidation of Fe in SS316

- Enhanced cation outward diffusion in metals that grows mainly by inward oxygen transport (better balance in the oxide growth)
- Up to a certain concentration, H in stainless steel S 35315 increases the resistance to localized corrosion in chloride solutions
- Up to a certain concentration, H reduces the oxidation rate of Zr in O_2 at 400°C
- Enhances the oxidationof As in GaAs

Most of the above-mentioned processes take place at high temperatures. A thermodynamic approach for the analysis of possible sources and sinks of hydrogen at various temperatures is also presented. The effect of the porosity on the hydrogen uptake is analysed for pretransition oxide scales on a Zr-based alloy.

4.5 Paper V

A gas phase analysis technique applied to in-situ studies of gas-solid interactions

In **Paper V**, a description of an ultrahigh vacuum technique using mass spectrometry for in-situ investigations of gas-solid interactions is presented.

The following types of investigations are presented with some examples:

- Studies of *gas uptake kinetics in solids* exemplified by the oxidation of pure Fe and a Zr-based alloy in oxygen gas,
- *Isotopic exchange studies* exemplified by O_2 dissociation on the surface of a wide range of solid materials,
- *Outgassing studies* exemplified by outgassing of an air equilibrated oxide layer on Zircaloy-2, and
- *Permeation of gases through oxide membranes* exemplified by oxygen permeation through a 2mm thick zirconia membrane.

Gas Phase Analysis (GPA) technique is a useful tool to characterize complex processes, identify and characterize reaction mechanisms and transport properties of a wide range of materials. In-situ information is obtained by combining manometric and mass spectrometric data. A complementary isotopic sensitive technique such as Secondary Ion Mass Spectroscopy (SIMS) can be used to characterize the reaction products. The GPA technique can be used at temperatures from room temperature to 1200°C and at pressures up to 1 atm. Aspects related to sample preparation, isotopic gas mixture selection, data acquisition, calibration and interpretation of the experimental data are also addressed.

4.6 Paper VI

Isotopic investigation of the transport of oxygen species in Y-stabilized zirconia

Oxygen transport in commercial sintered zirconia ceramics was investigated at temperatures between 400 and 900°C using labeled oxygen gas mixtures in combination with permeation and uptake-release types of measurements. The aim of the paper is to clarify the contribution of the molecular transport to the total oxygen transport (ions, atoms and molecules) in Y-stabilized zirconia (YSZ).

1. Uptake-release measurements

A polycrystalline Y-stabilized $Zr^{16}O_2$ (YSZ) tube (outer diameter = 7 mm, inner diameter = 5 mm, length = 150 mm) was exposed to $^{18,18}O_2$ gas at temperatures between 600 and 900°C followed by outgassing at the respective temperatures. During the exposure, the uptake of oxygen by YSZ was quantified by measuring the pressure decrease in the reaction chamber. The composition of the gas phase was continuously analyzed with a mass spectrometer placed in an UHV chamber via a leak valve. The results show that:

- The oxygen exchange ($^{18,18}O_2 \Leftrightarrow Zr^{16}O_2$) rate exceeds the oxygen uptake rate in YSZ only at temperatures above 700°C.
- At low temperatures, a considerable molecular oxygen transport is operative in YSZ.

2. Permeation measurements

A Y-stabilized $Zr^{16}O_2$ tube (outer diameter = 12 mm, inner diameter = 8 mm, length = 250 mm, wall thickness = 2 mm) was used as a membrane tube. The permeation experiments have been performed using two different gas mixtures, i) ^{18}O-containing oxygen gas and ii) a gas mixture with the composition of 25%He, 25%Ar, 25% N_2 and 25% O_2.

The results show that:

- The oxygen exchange rate is crucial for the incorporation of the O^{n-} species into the oxide lattice. Low exchange rates therefore result in low O^{n-} contribution to the net oxygen flux through the membrane. This is valid for YSZ at temperatures up to 800°C.
- Oxygen molecules are indeed involved in the total oxygen transport in YSZ with a considerable contribution at temperatures below 800°C.
- In the permeated gas detected upon permeation of 1 atm. mixed gas (25%He, 25%Ar, 25% N_2 and 25% O_2) through YSZ tube at 200°C, the transport of He, N_2 and O_2 have been identified.

Possible measures for maximization of the transport of the dissociated oxygen species in YSZ are suggested.

Chapter 5

Conclusions

The results obtained using isotopic gas mixtures and isotope-monitoring techniques such as Gas Phase Analysis and Secondary Ion Mass Spectrometry have opened new perspectives for the understanding of phenomena involved in the transport of hydrogen and oxygen species in oxide scales on Zr-based alloys. The following main conclusions have been drawn:

- Modification of the oxide surface properties (oxide/gas interface) can influence the **inward transport** of species such as hydrogen and oxygen. Two main effects were distinguished:
  - ***Inhibitor effect***: CO is identified as an effective site blocker for hydrogen adsorption and dissociation on preoxidized Zircaloy-2 at temperatures around 400°C. No influence of N_2 on the hydrogen uptake in Zircaloy-2 is found. Based on the results of the present work, the following rating for the tendency for adsorption on oxidized Zircaloy-2 and Cr_2O_3 in the temperature range of 400-600°C was made: $N_2 < H_2 < CO < H_2O$.
  - ***Catalytic effect***: porous Pt coated on the Zr surface, catalyses oxygen dissociation at the gas/oxide interface, promoting inward oxygen transport. At 400°C, oxygen dissociation efficiency decreases in the order: Pt > Zr_2Fe > Zr_2Ni > $ZrCr_2$ ≥ Zircaloy-2.
- Modification of the oxide/metal interface can influence the **outward transport** of cations. Enhanced outward diffusion of Zr^{4+} cations induced by the presence of hydrogen at the oxide/metal interface and inside the oxide scale has been identified.
- ***Self-repairing effect:*** An improved **balance** in the oxide growth on Zr was obtained by combining the effect of Pt (enhanced inward oxygen transport) and D (enhanced outward Zr diffusion). As a result, a more protective oxide layer was formed.
- We propose that Fe-containing second-phase particles act as oxygen dissociating elements in an analogue way as Pt. Hence, a proper choice of second-phase particles in terms of composition and size distribution can be beneficial for reducing the negative effect of hydrogen uptake at high concentrations.
- Open porosity with effective pore diameters in nanometer range have been found in thermally-grown pretransition oxide scales on Zircaloy-2.
- In commercial sintered Y-stabilized zirconia ceramics, a considerable contribution of molecular transport to the total oxygen transport has been found at temperatures up to 800°C

Chapter 6

Future work

Hydrogen is quite an exciting small molecule, which generates important technological problems. Further investigations of the hydrogen transport in oxides needs to be considered. One question arises: Can atomic and/or molecular hydrogen be transported through the zirconia layer, and under which conditions? The results presented in this thesis show that an open porosity in nm-range is present in pretransition oxides on Zircaloy-2. These pores can accommodate without doubt molecular species like hydrogen and/or water.

Formation of hydrides is also an important issue that needs to be further clarified. In hydrides, hydrogen is negatively charged. To form hydride ions inside an oxide, special reducing conditions are necessary. Close to the oxide/metal interface, these reducing conditions are possible to appear, and thus, the oxide becomes thermodynamically unstable, oxygen can dissolve in the metal underneath the oxide, and hydrides start to from. The formation of "substitutional hydroxides" could be the prerequisite for hydride formation inside the oxide layer. Further studies related to the effects of hydrogen on the properties of oxides would be of much interest.

Optimisation of transport properties of oxides (nanomaterials) by engineering of interfaces and surfaces is an area, which can be further developed.

Chapter 7

Acknowledgments

There are many people that I would like to thank for helping me in many ways:

First of all, I would like to thank to my supervisor, ***Doc. Gunnar Hultquist***, for introducing me into the fascinating world of the isotopic measurements and for sharing with me valuable knowledge. Thank you for the scientific support and for the stimulating working atmosphere.

I am grateful to ***Prof. Christofer Leygraf***, for his guiding and moral support in difficult moments. Thank you for the fruitful discussions and for your enthusiasm and inspiration.

Many warm thanks to ***Magnus Limbäck***, my supervisor from Westinghouse Electric Sweden AB, for organising this project and for all the professional and personal support. Thank you for your kindness and friendship.

Very special thanks to ***Ass. Prof. Inger Odnevall Wallinder,*** for her kindness and for giving me encouragement and friendship as well as for having always a good advice when I needed. Thank you for reviewing my manuscript and for all the valuable suggestions. Great thanks for all the personal and professional support.

Warm thanks to ***Erik Hörnlund*** for sharing his passion for computers with me, for showing me tricks and tips about animations and for all his professional help.

Great thanks to ***Dr. John Rundgren*** for his suggestions about animations and for sharing with me his knowledge about diffusion.

I wish to express my gratitude to all ***Zr Experts Group Friends*** for interesting discussions and scientific advice.

I gratefully acknowledge ***Doc. Gunnar Wikmark*** at Studsvik nuclear, for being such a great opponent for my licentiate defence and for giving me valuable advice, guidance and inspiration

Warm thanks to ***Prof. Elisabeth Ahlberg*** at Göteborg University and ***Prof. Bevis Hutchinson*** at KIMAB for the fruitful discussions.

Thanks also to ***Mats Dahlbäck*** and ***Per Tägtström*** for the valuable suggestions.

I would like to show my deepest gratitude to ***Dr. Isao Saeki*** at Muroran Institute of Technology, Hokkaido, Japan for the excellent collaboration, for the stimulating discussions and for the great time during the High Temperature Corrosion Symposium in Japan. Warm thanks also to ***Prof. Shigeji Taniguchi*** at Osaka University, Japan.

I have really enjoyed the time together with all my past and present collegues and friends at the Corrosion Division.You made these 4.5 years an unforgettable experience! ***Anna***, thank you for being such a great friend and a very special person. During these years we had such a wonderful friendship and I cannot thank you enough for all your support and encouragement! Warm thanks

also to ***Jonas***. ***Klara***, thank you for your friendship and never ending optimism. ***Andreas*** and ***Janne***, thank you for being really nice roommates and friends. Thanks for correcting my Swedish and practicing it with me! Special thanks to ***Johan***, my "high temperature corrosion" friend, for his companionship and inspiration. Many warm thanks to ***Ali Davoodi*** for all the AFM measurements and for being a good friend. ***Sofia, Gunilla***, ***Babak***, ***Jonas*** and ***Harveth***, thank you for the friendly atmosphere and the great time at Korrosionslära and also outside the office. ***Jinshan*** and ***Bo*** thanks for the suggestions and exciting discussions. Great thanks to ***Peter Szakalos,*** for all his help with the SEM and LOM and also for the exciting and stimulating discussions. ***Sara***, thank you for the relaxing trips and exciting tours.

I am grateful to ***Prof. Arthur Motta*** at The Penn State University, USA for the stimulating discussions and suggestions.

Prof. Mike Graham at The National Research Council of Canada is gratefully acknowledged for the fruitful discussions, suggestions and for the great karaoke duet.

Financial support from ***Westinghouse Electric Sweden AB*** is gratefully acknowledged.

I would like to show my sincerest gratitude to my Romanian mentors who have inspired me over the years and shared with me their knowledge: ***Prof. Cristina Nemes Bota***, ***Conf. Univ. Dr. Gabriela Oprea***, ***Dr. Manuela Hagiopol***, ***Prof. Virginia Burghelea*** and ***Prof. Ecaterina Andronescu***. Va multumesc ca ati fost alaturi de mine si mi-ati indrumat pasii de-alungul anilor!

I am very grateful to my friends, ***Petre***, ***Mona***, ***Meli***, ***Manish*** and ***Karl*** for the great time spent together. Warm thanks also to all my close ***friends*** from far distance at the Institute for Nuclear Research, Pitesti, Romania.

I wish to thank my entire family for providing a loving environment for me, my sisters ***Ildiko*** and ***Agi***, my brothers ***Zoli*** and ***Radu***, my mother ***Agneta*** as well as my parents in law, ***Maria*** and ***Petre***. I would like to dedicate this thesis to a very special person, my father, who is not with us anymore. Life is sometimes too short!

Finally, and most importantly, ***Ionut*** thank you for your true love and endless concern, emotional support and for your patience. You are a great partner and a very special person!